Supporting Information

An intramolecular cobalt-peptoid complex as an efficient electrocatalyst for water oxidation at low overpotential

Suraj Pahar and Galia Maayan*

Schulich Faculty of Chemistry, Technion-Israel Institute of Technology, Technion City,

Haifa 3200008, Israel. E-mail address: gm92@technion.ac.il.

Experimental Procedures

Materials

Rink Amide resin was purchased from Novabiochem; benzylamine, ethanolamine and 6-bromo-2,2′-bipyridine were purchased from Acros organics, Israel; N,N′-diisopropylcarbodiimide (DIC) and bromoacetic acid were purchased from Sigma Aldrich. 4'-Chloro-2,2':6',2''-terpyridine and TFA were purchased from Alfa Aesar. 2-(4'-Chloro-2,2':6',2''-terpyridine-4'-yloxy) ethylamine and 2-(2,2'-bipyridine-6-yloxy) ethylamine were prepared according to a literature method [1,2] and –OH group of ethanolamine was protected using a reported procedure[3]. The purchased reagents, solvents, and HPLC grade reagents were purchased from commercial sources and used without further purification, except for DMF that was dried with molecular sieves. The used solvents were HPLC grade. High purity deionized water was obtained by passing distilled water through a nanopore Milli-Q water purification system. Aqueous phosphate buffer solutions were prepared using specific concentrations of mono, di- and tribasic phosphate salts with added 0.1 M NaOH solution such that the final ionic strength was 0.1 M.

Instrumentation

Peptoid oligomers were analyzed by reversed-phase HPLC (analytical C18 column, 5μm, 100Å, 2.0 x 50 mm) on a Jasco UV-2075 instrument. A linear gradient of 5–95% ACN in water (0.1% TFA) over 10 min was used at a flow rate of 0.7 mL/min. Preparative HPLC was performed using a phenomenex C18 column (15μm, 100 Å, 21.20x100mm) on a Jasco UV-2075 instrument. Peaks were eluted with a linear gradient of 5–95% ACN in water (0.1% TFA) over 50 min at a flow rate of 5 mL/min. Mass spectrometry was performed on Advion expression mass under electrospray ionization (ESI), direct probe ACN: H_2O (70:30), flow rate 0.3 ml/min. UV-Vis measurements were recorded on an Agilent Technologies Cary 60 UV-Vis spectrophotometer using a 1 cm path length quartz cuvette. IR spectra (400-4000 cm^{-1}) were recorded on an Agilent Cary 630 FTIR spectrometer, equipped with a diamond attenuated total reflection (ATR) instrument, which allows direct measurement with no sample preparation. EPR spectra were obtained on a Bruker EMX-10/12 X-band (ν = 9.2 GHz) digital EPR spectrometer equipped with a Bruker N_2 temperature controller. Samples were irradiated with the focused and filtered (λ = 300 nm) light of a high-pressure mercury lamp (1 kW) (ARC

lamp power supply model 69920) in the resonator of EPR spectrometer. All spectra were recorded at a non-saturating microwave power of 200mW, 100 kHz magnetic field modulation of 1 G amplitude. Spectra processing and simulation were performed with a Bruker WIN-EPR and SimFonia Software. Scanning electron microscopic (SEM) images were taken from TESCAN VEGA Nanospace instrument. ^{1}H-NMR spectra were recorded using an AVANCE II 400 MHz Bruker spectrometer.

Electrochemical Methods

Cyclic voltammetry (CV) and differential pulse voltammetry (DPV) experiments were carried out on EmStat PalmSens electrochemical analyzer in a three-electrode system containing Glassy Carbon (GC) as working electrode, Ag/AgCl as reference electrode and Pt wire as counter electrode. Before each measurement, the working electrode was polished with 0.05 μm alumina paste followed by rinsing with water and finally drying in air. All redox potentials in this work have been reported versus NHE by adding 0.197 V to the measured potential. CVs were collected at 100 mV/s except for other specifications. DPV was obtained with the following parameters: Amplitude = 200 mV, E-step = 10 mV, pulse width = 0.01 s.

O_2 evolution experiment

Controlled Potential Electrolysis (CPE) experiments were performed using a two-compartment cell closed with septum. Large surface porous carbon (spongy shape) as working electrode together with a Ag/AgCl (NaCl sat.) as reference electrode was placed in one of the compartment that was filled with a 0.5mM buffer solution of the catalyst (pH 7, phosphate buffer 0.1 M of ionic strength). In the other compartment, containing only the buffer solution, a mesh platinum counter electrode was used. Before starting the experiment, nitrogen gas was purged for 10 min to remove the oxygen from the system. Oxygen evolution was monitored in the gas phase with a Fixed Needle-Type Oxygen Minisensor (from PyroScience) placed in the headspace of the reaction vassal (working electrode side). The CPE started as soon as the oxygen sensor signal was stable. During the experiment, solutions of both compartments were vigorously stirred. The results of the water oxidation catalysis with cobalt complex compared with the blank experiment in the same conditions but in the absence of the catalyst. The Faraday efficiency was determined according to the total charge passed during the CPE and the total amount of generated oxygen by considering that water oxidation is a 4-electron oxidation process. The oxygen was measured by the oxygen sensor in % and converted to μmol using a calibration curve. This was constructed by the gradual addition of the known amount of pure oxygen (μL) into the cell containing buffer solution using a Hamilton syringe while measuring the oxygen in % by the oxygen sensor and then by plotting the amount of pure oxygen added (μL) vs. the amount of oxygen (%) shown by oxygen sensor to get the total amount of oxygen evolved in μL during electrolysis (Figure S70). This was further converted to μmol via the equation: y μmol = x μL/(24.5 L/mol), T = 298 K.

Calculation of Faradic Efficiency from total charge accumulated during Control Potential Electrolysis (CPE): -

Faradic efficiency (FE (%)) was calculated based on following equation:

$$\text{FE (\%)} = \frac{4\ x\ amount\ of\ oxygen(moles)\ x\ 100}{n\ (moles\ of\ electrons)}$$

$$\text{Where, n} = \frac{Q\ (Columb)}{F\ (Faraday\ const.)}$$

Preparation and Characterization of Peptoids Oligomers

The peptoids **TBE** were synthesized manually on Rink amide resin using the sub-monomer approach[4]. In a typical synthesis, rink-amide resin (100 mg) was measured and swallowed in DCM for a period of 40 minutes. De-protection of the resin was carried out by piperidine solution (20%, solvent: DMF) followed by 20 minutes shaking in ambient condition. Next, piperidine was washed by DMF for three times with one minute duration (1 mL/ 25 mg resin each time). Bromoacetylation was done by addition of 20 eq. Bromoacetic acid (1.2 M in DMF, 8.5 mL/g resin) together with 24 eq. of diisopropylcarbodiimide (2 mL g-1 resin), shaking for 20 min in room temperature. Afterwards, the bromoacetylation reagents were properly washed from the resin by DMF (1 mL/ 25 mg resin each time, three times with one minute duration each time). After washing, 20 eq. of the primary amine (1.0 M in DMF, 10 mL/g resin) was added under shaking for next 20 minutes at room temperature except for 2-(2,2' :6',2"-Terpyridine-4'-yloxy) ethylamine and 2-(2,2'-bipyridine-6-yloxy) ethylamine for 5 hours and later washed three times by DMF. Bromoacetylations and amine displacement steps were repeated till the desired sequence was loaded on the resin. Following the reaction, the resin was washed by DCM three times and the peptoids were cleaved from the resin by 95% TFA in water (40 mL/g resin) for 20 minutes. The cleavage cocktail was evaporated under low pressure, solubilized in 5 mL HPLC grade solvent 1:1 acetonitrile: water mixture and lyophilized overnight. The peptoids were further purified to >95% by RP-HPLC and lyophilized overnight. The peptoids after purification were characterized by analytical HPLC and ESI-MS analysis.

Synthesis of complex Co**TBE:**

The peptoid **TBE** (1M in MeOH) was treated with 1 molar equivalent of cobalt acetate tetrahydrate ($Co(CH_3COO)_2 \cdot 4H_2O$) in MeOH was added and the mixture was allowed to stir for 2 hours. The formed complex was precipitated using excess sodium perchlorate ($NaClO_4$) and centrifuged for 10 minutes. Then the excess solution was removed. The solid complex was purified by washing with cold MeOH (2 ml × 5-6 times) until the solvent became colorless. The metal complexes were analyzed by ESI-MS, UV-Vis spectroscopy, EPR, ^{1}H-NMR and FTIR.

Supplementary Figures

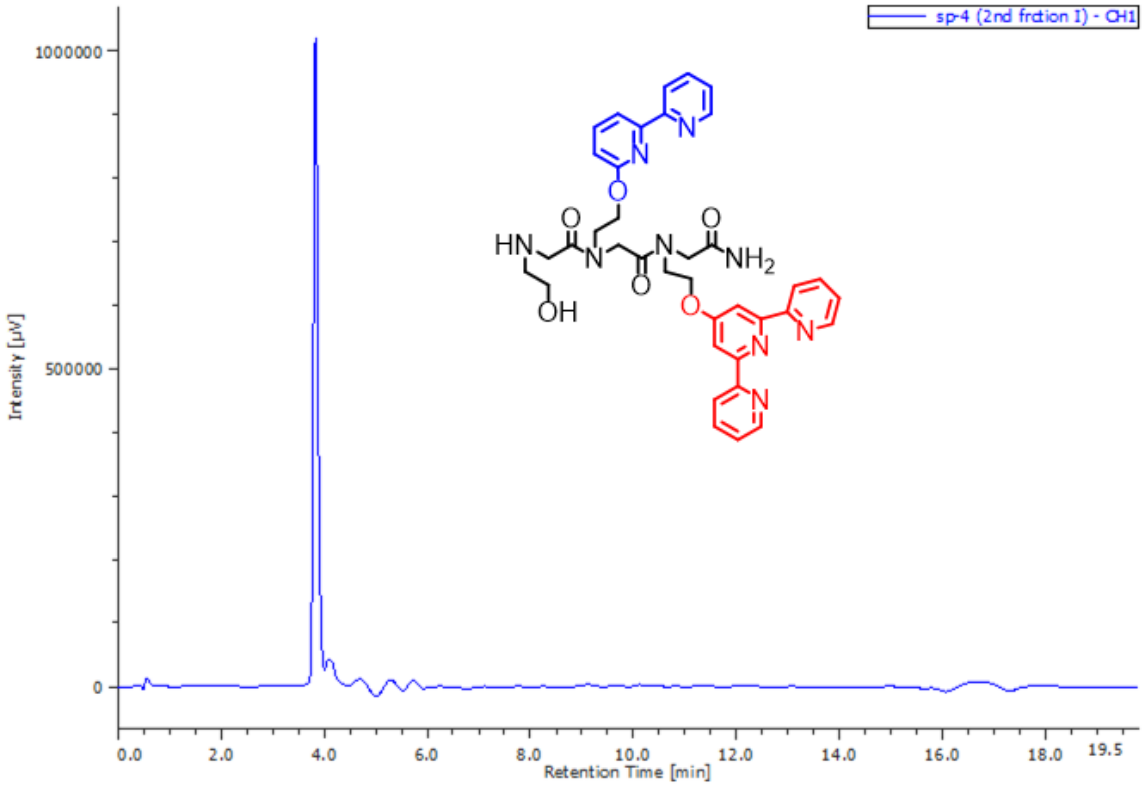

Figure S1. HPLC traces of pure peptoid **TBE**.

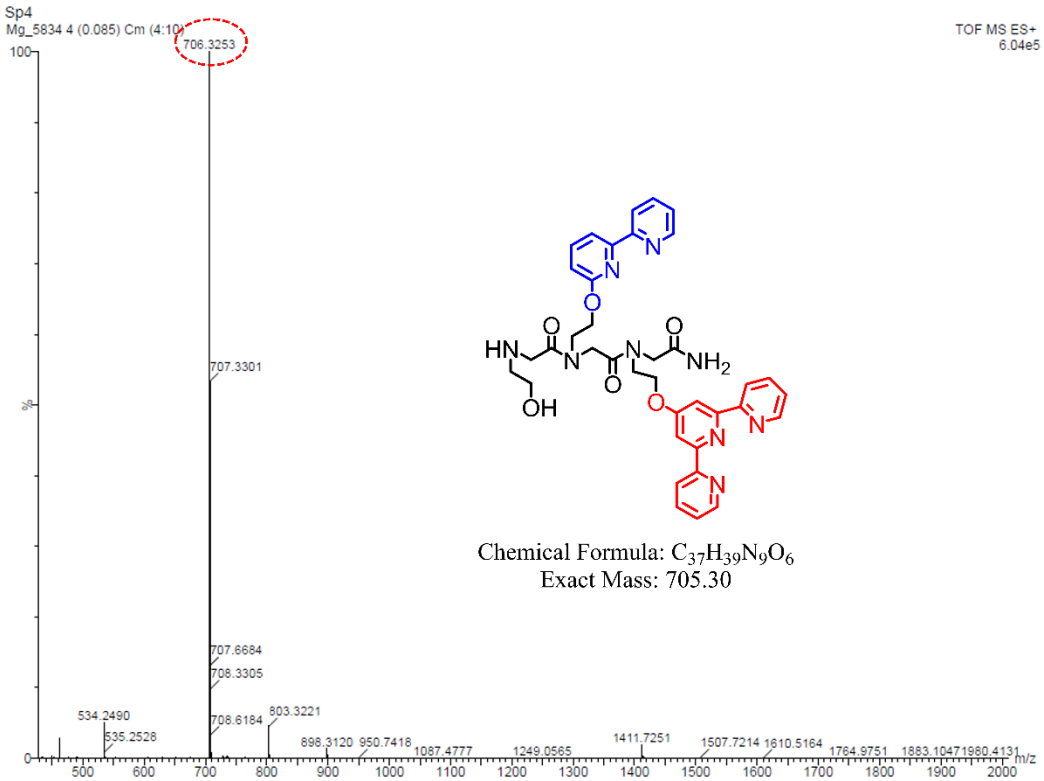

Figure S2. High-resolution ESI-MS of peptoid **TBE** in acetonitrile, m/z (**TBE** + H^+) = 706.32.

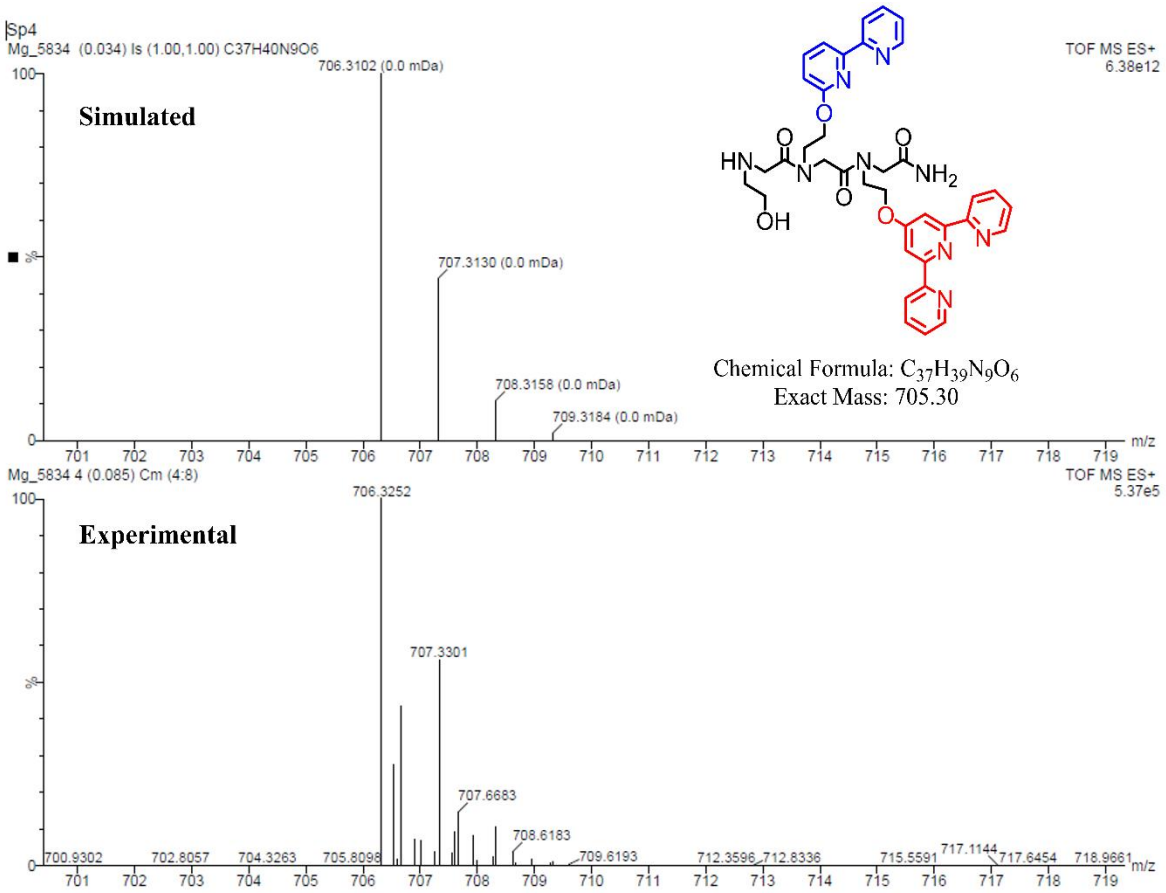

Figure S3. High-resolution ESI-MS of **TBE** in acetonitrile; (simulated & experimental mass of m/z (**TBE** + H^+) = 706.32).

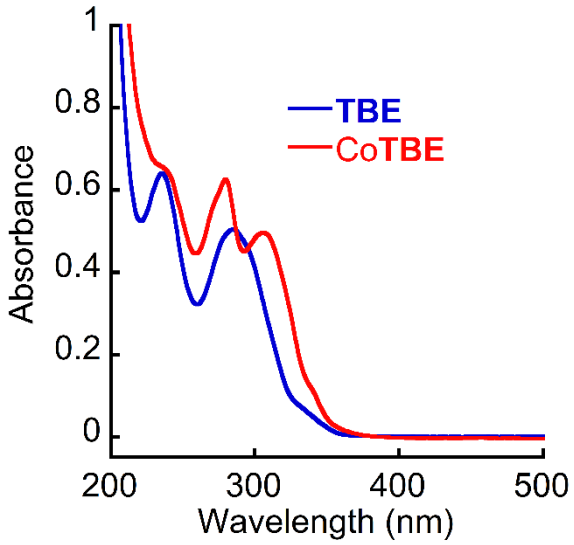

Figure S4. UV-Vis spectra of ~25 µM of the peptoid **TBE** and complex Co**TBE** in 0.1 M PBS at pH 7.

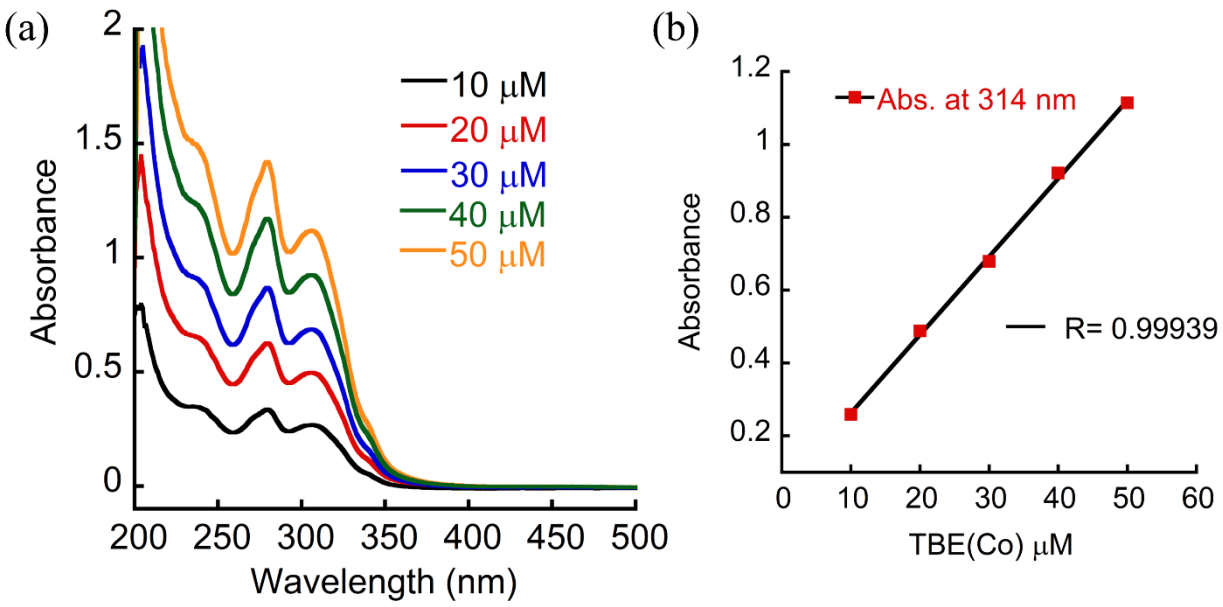

Figure S5. (a) UV-Vis spectra of complex Co**TBE** with different concentrations in 0.1 M phosphate buffer at pH 7. (b) Plots of the absorption intensity at λ = 314 nm as a function of Co**TBE** concentration.

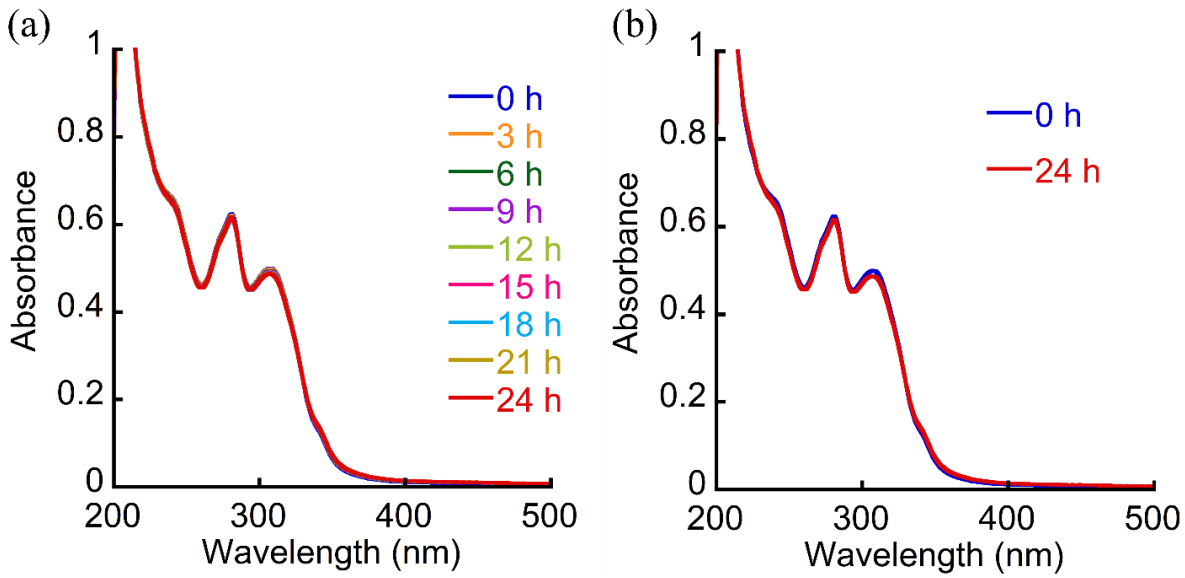

Figure S6. UV-Vis absorption spectra of ~25 μM of Co**TBE** in 0.1M phosphate buffer at pH 7 without disturbing for 24 hours.

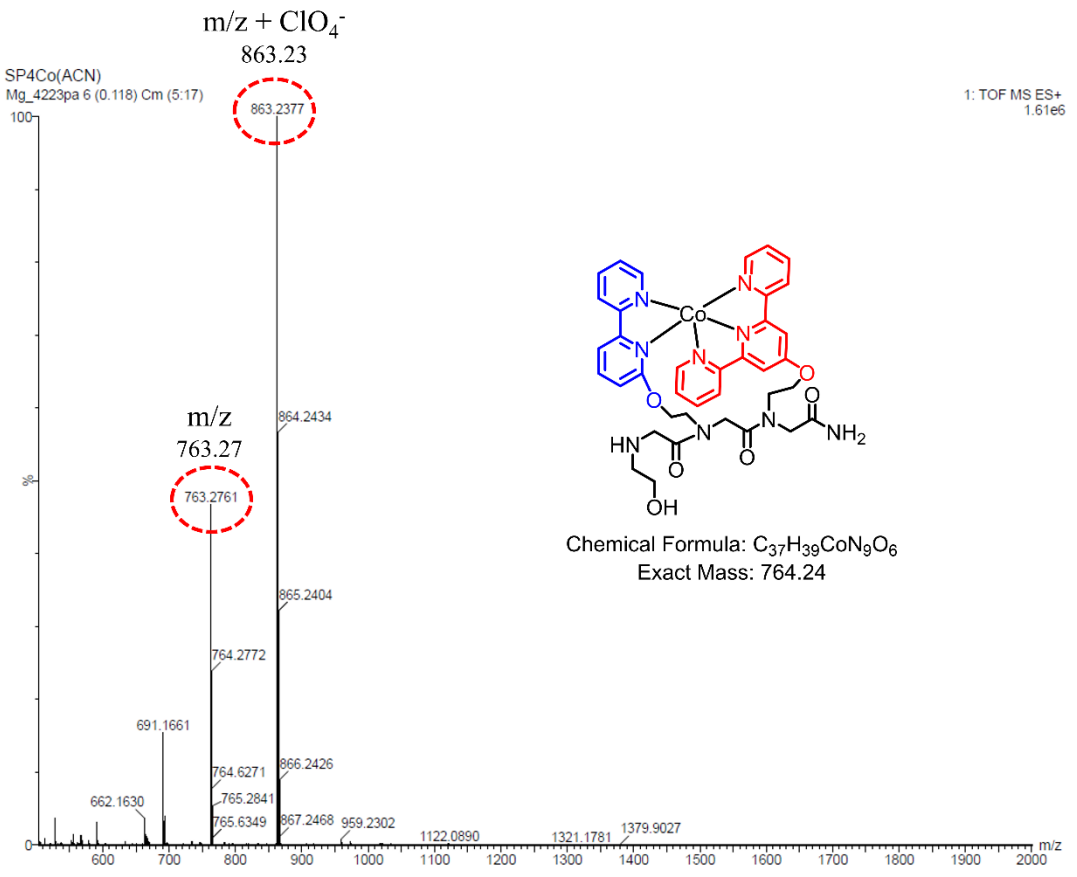

Figure S7. High-resolution ESI-MS of Co**TBE** in acetonitrile.

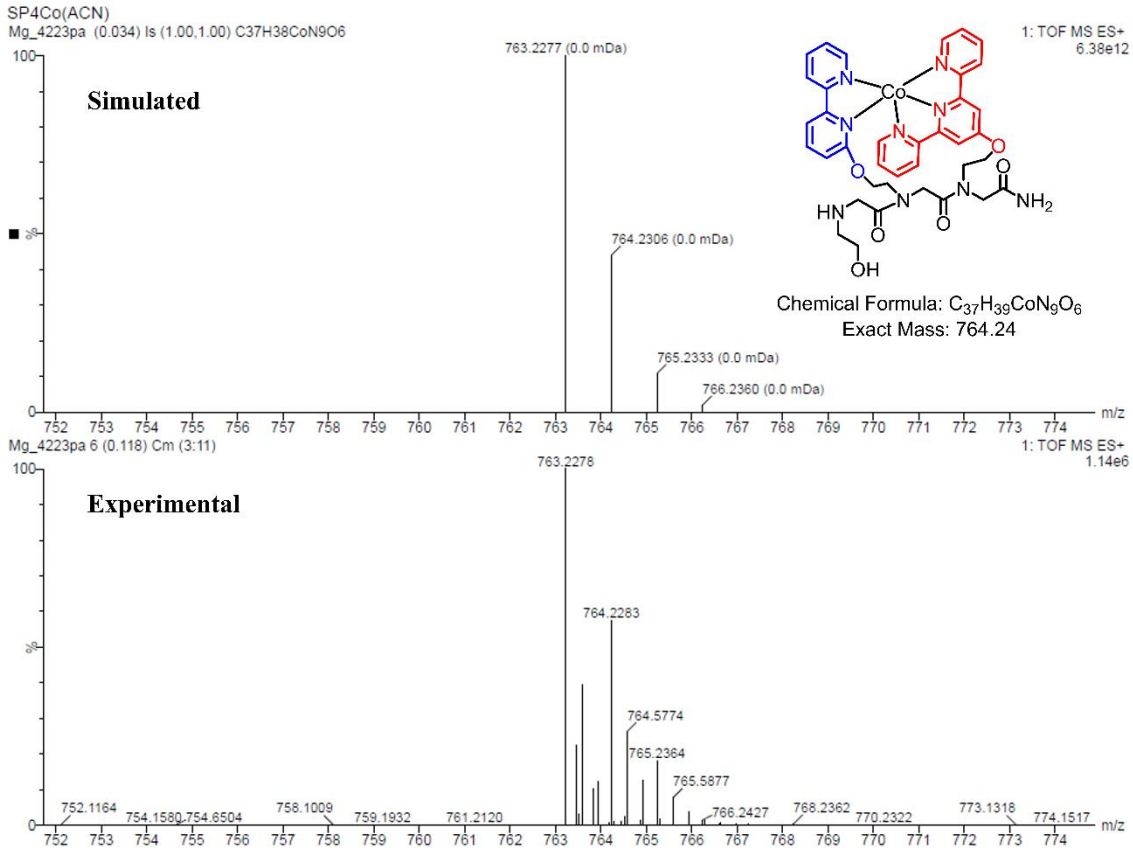

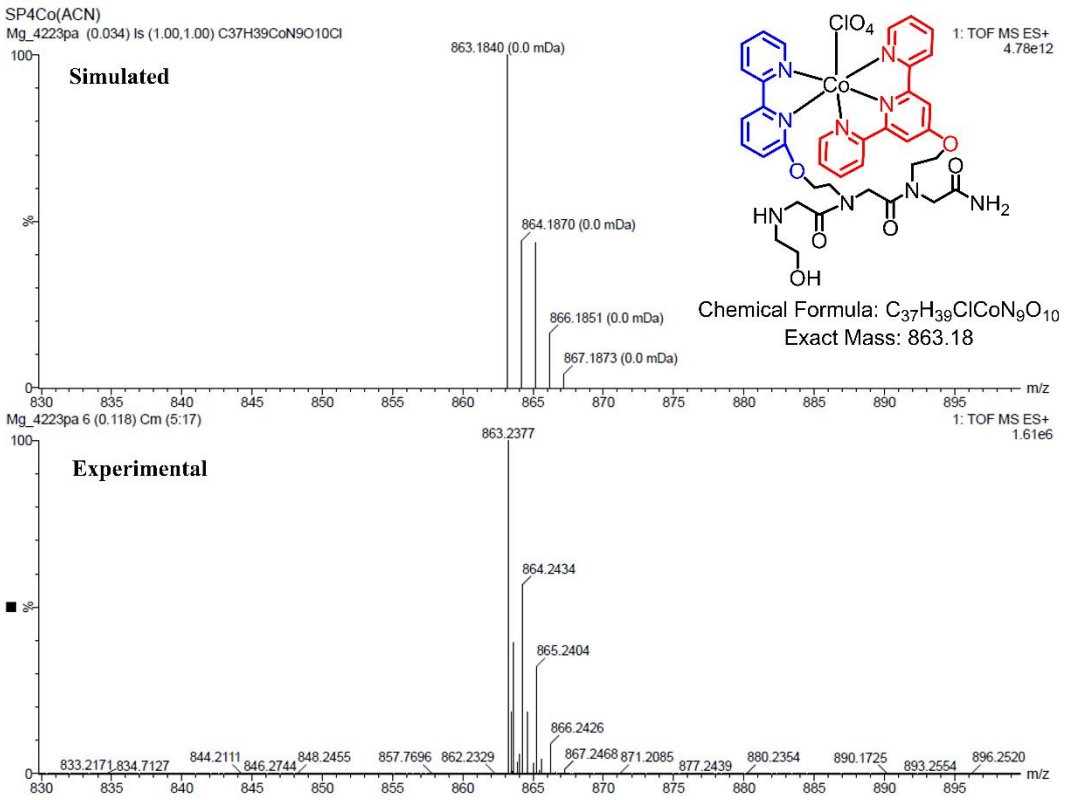

Figure S8. High-resolution ESI-MS of Co**TBE** in acetonitrile; (simulated & experimental mass).

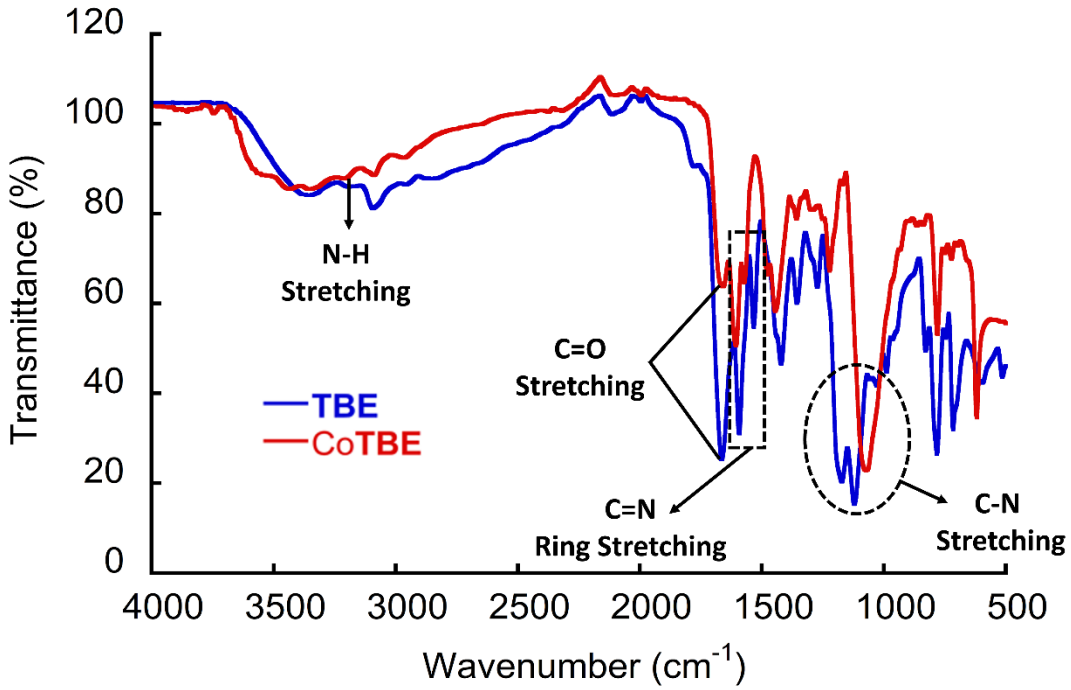

Figure S9. Solid-phase FT-IR spectra of **TBE** and its complex Co**TBE**. The black dashed circle indicates the shift in C-N stretching from 1121 to 1080 cm^{-1}, and the black dashed square

indicates the shift in C=N ring stretching from 1533 to 1571 cm^{-1}. No shifts were observed in the C=O (~1663 cm^{-1}) and N-H (~3206 cm^{-1}) stretching.

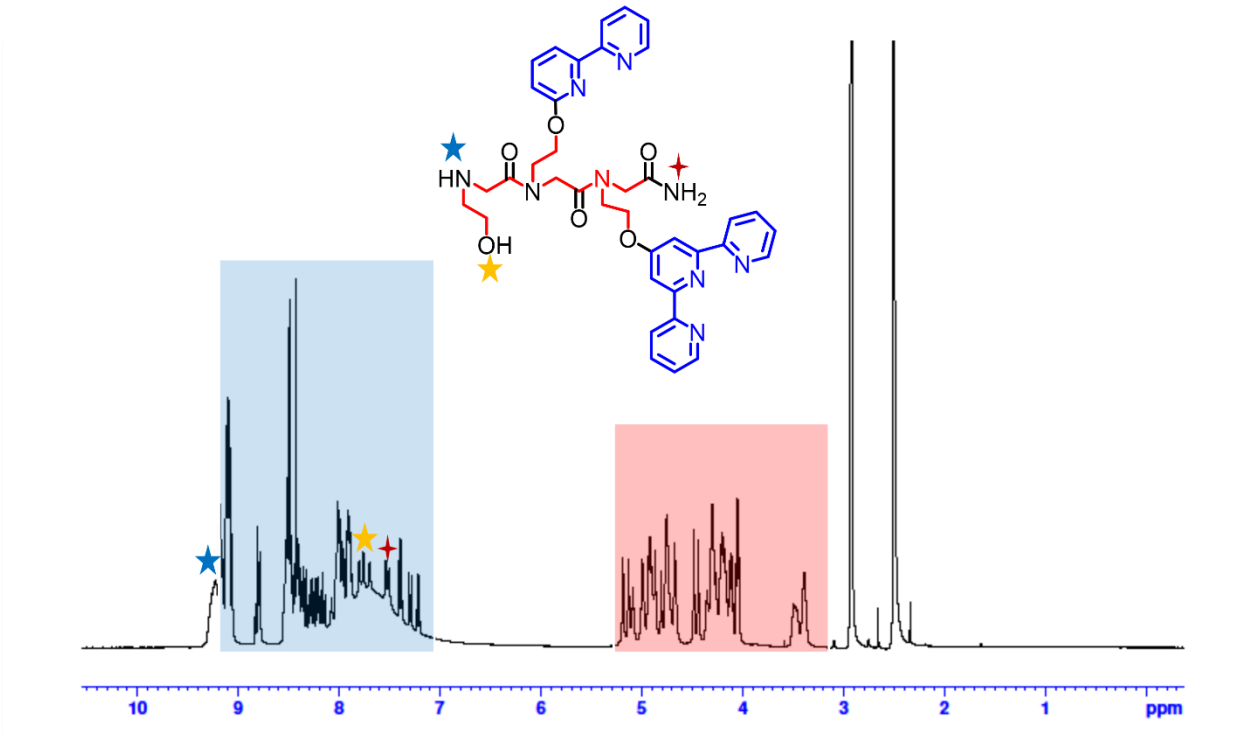

Figure S10. ^{1}H-NMR (in 400MHz) of peptoid **TBE** in DMSO-d6.

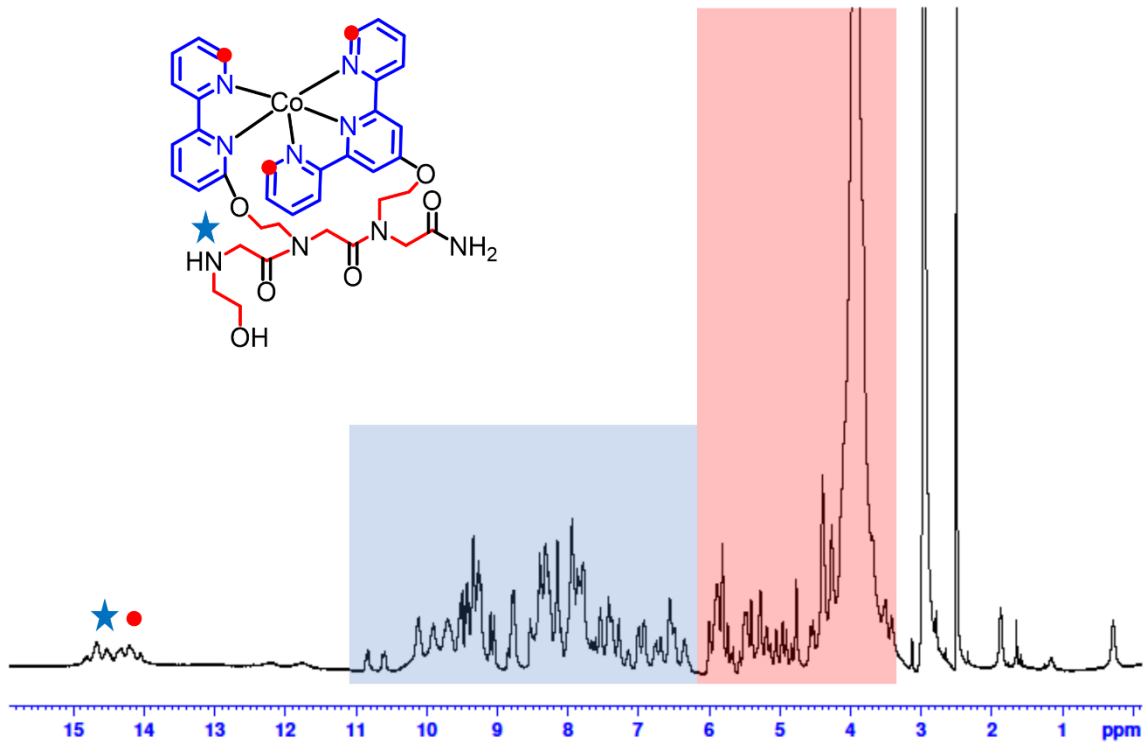

Figure S11. ^{1}H-NMR (in 400MHz) of peptoid Co**TBE** in DMSO-d6.

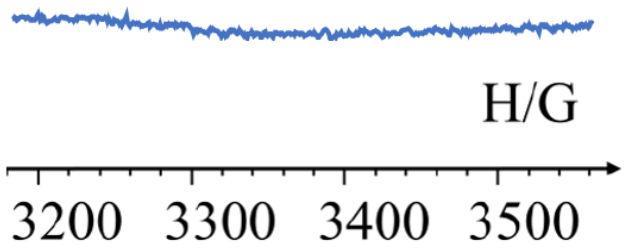

Figure S12. EPR spectrum of powder Co**TBE**. The silent EPR spectrum indicates that the cobalt ion is at Co(III) low-spin state. If it is Co(II) or Co(III) high-spin state, which is paramagnetic and then EPR spectrum is not silent.

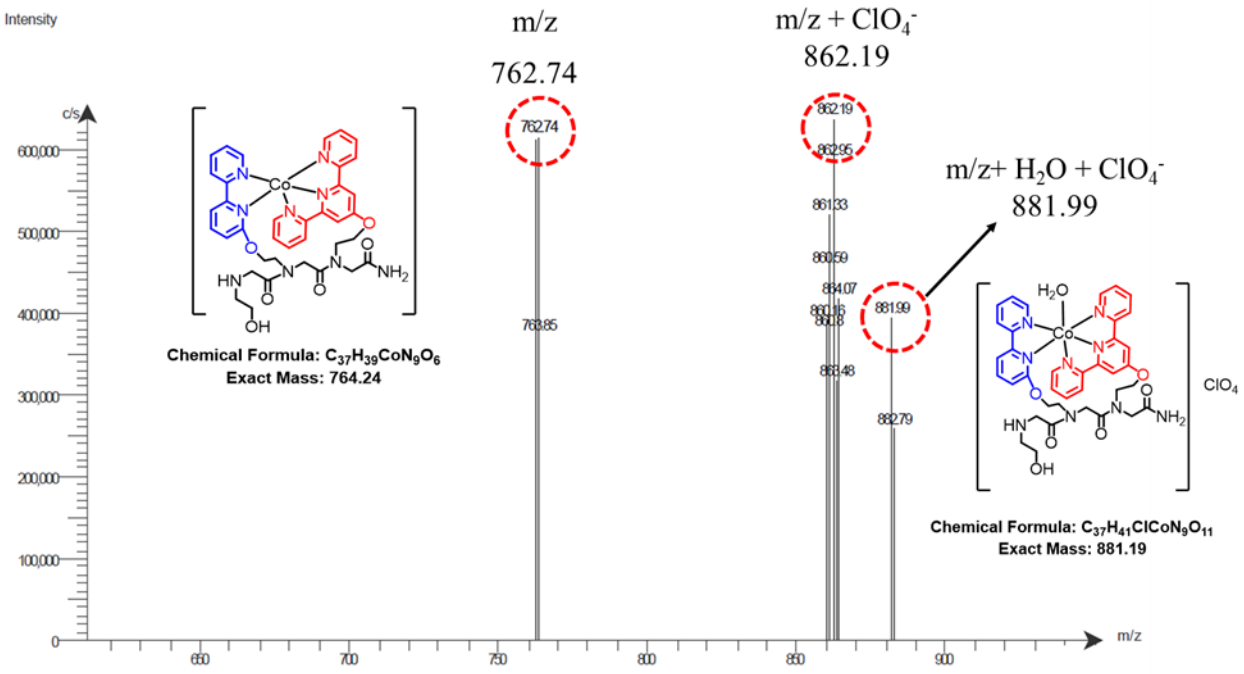

Figure S13. ESI-MS of Co**TBE** after a few hours in water.

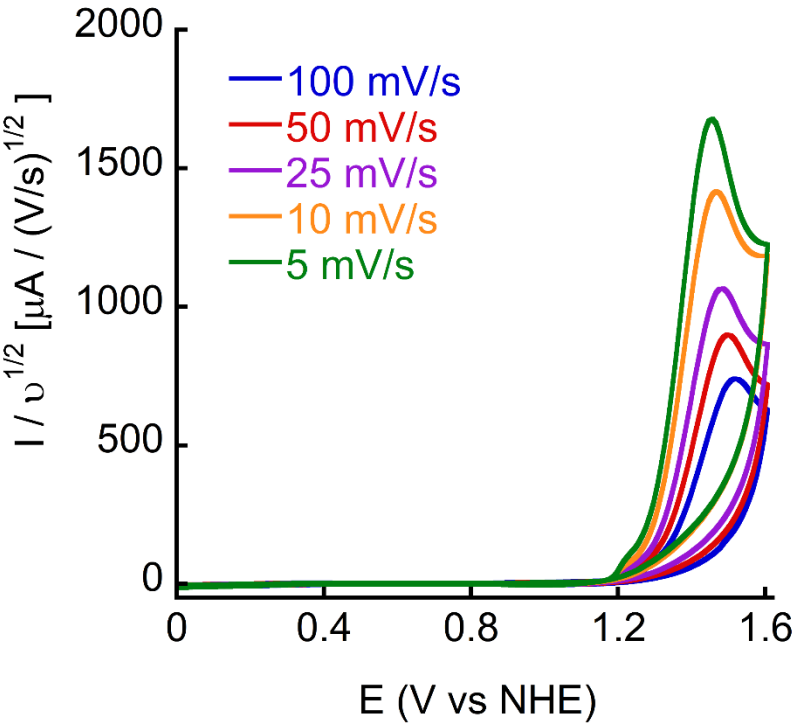

Figure S14. Scan rate normalized CVs of Co**TBE** in 0.1 M PBS at pH 7 using GC working electrode, Pt counter electrode and Ag/AgCl reference electrode.

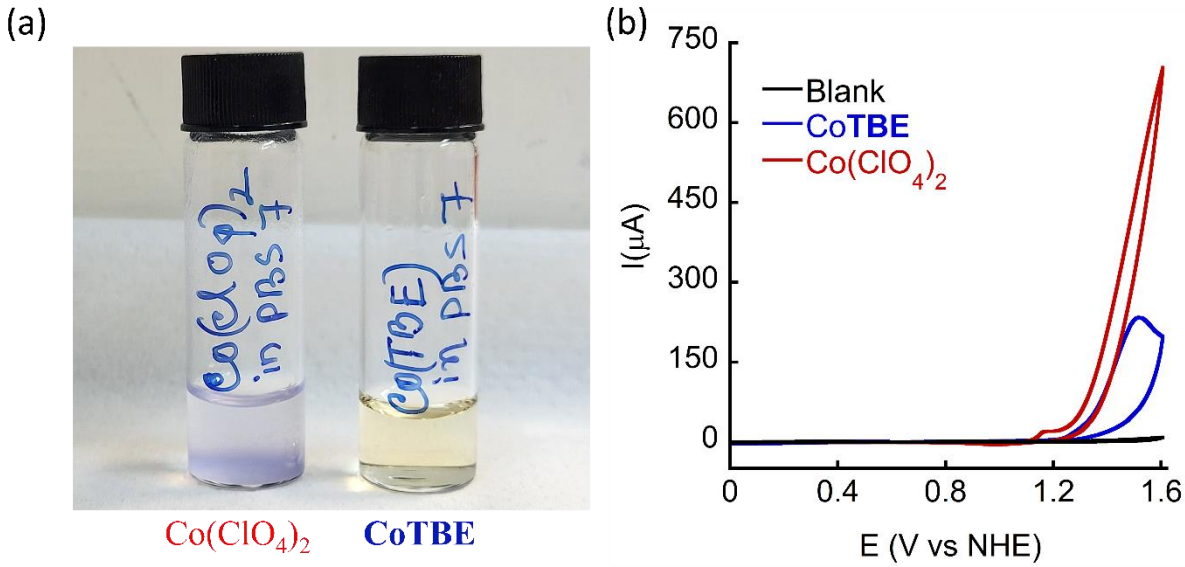

Figure S15. (a): ~ 0.5 mM $Co(ClO_4)_2 \cdot 6H_2O$ and 0.5 mM of Co**TBE** in 0.1 M phosphate buffer at pH = 7; (b) CVs of 0.1 M phosphate buffer solution at pH 7 with complex Co**TBE**, $Co(ClO_4)_2$, and without any catalyst (blank), scan rate = 100 mv/s.

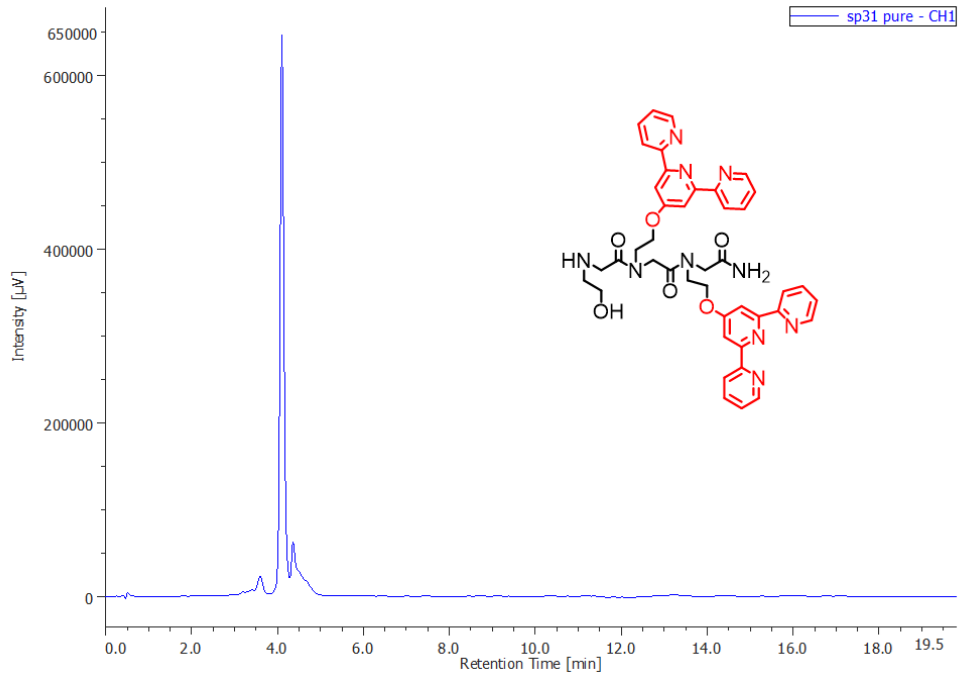

Figure S16. HPLC traces of pure peptoid **TTE**.

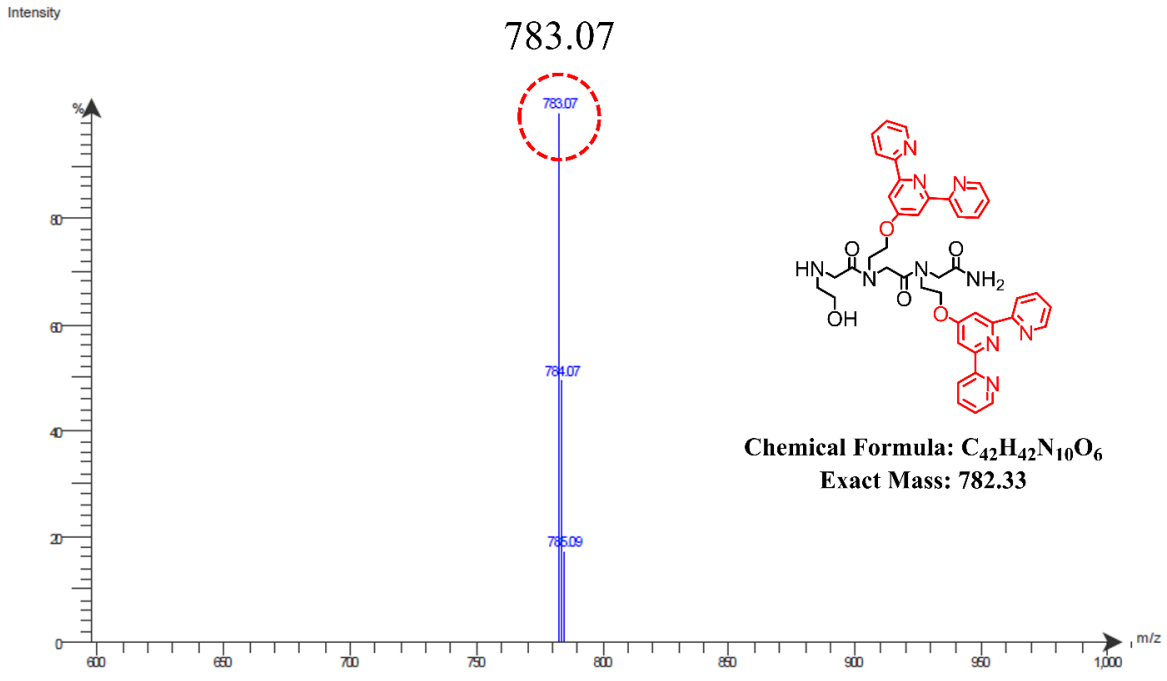

Figure S17. ESI-MS of peptoid **TTE**.

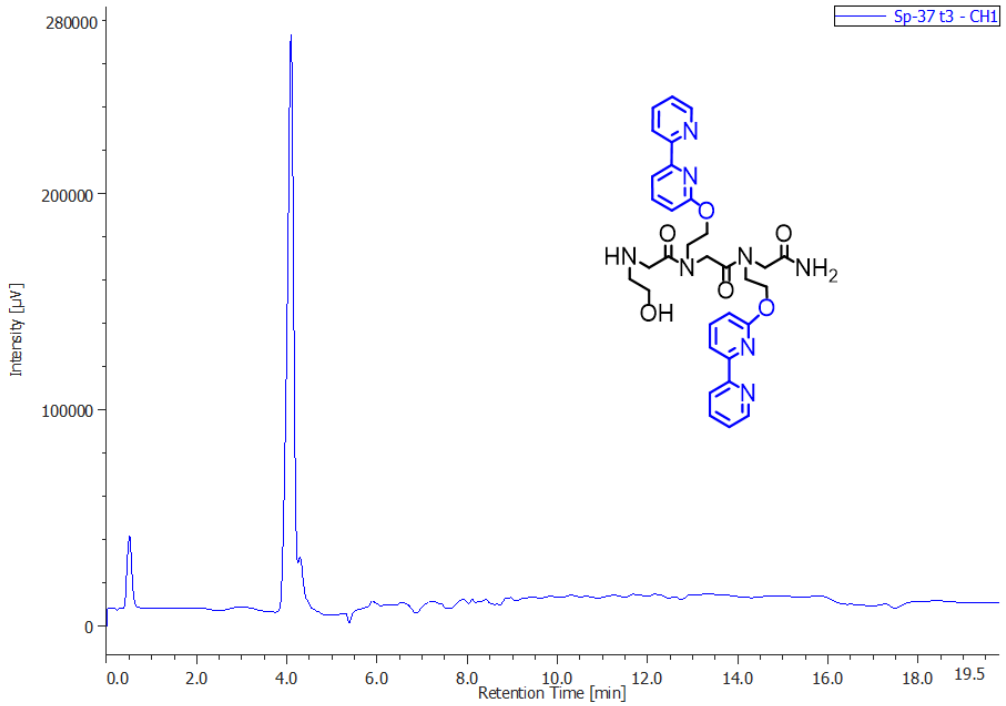

Figure S18. HPLC traces of pure peptoid **BBE**.

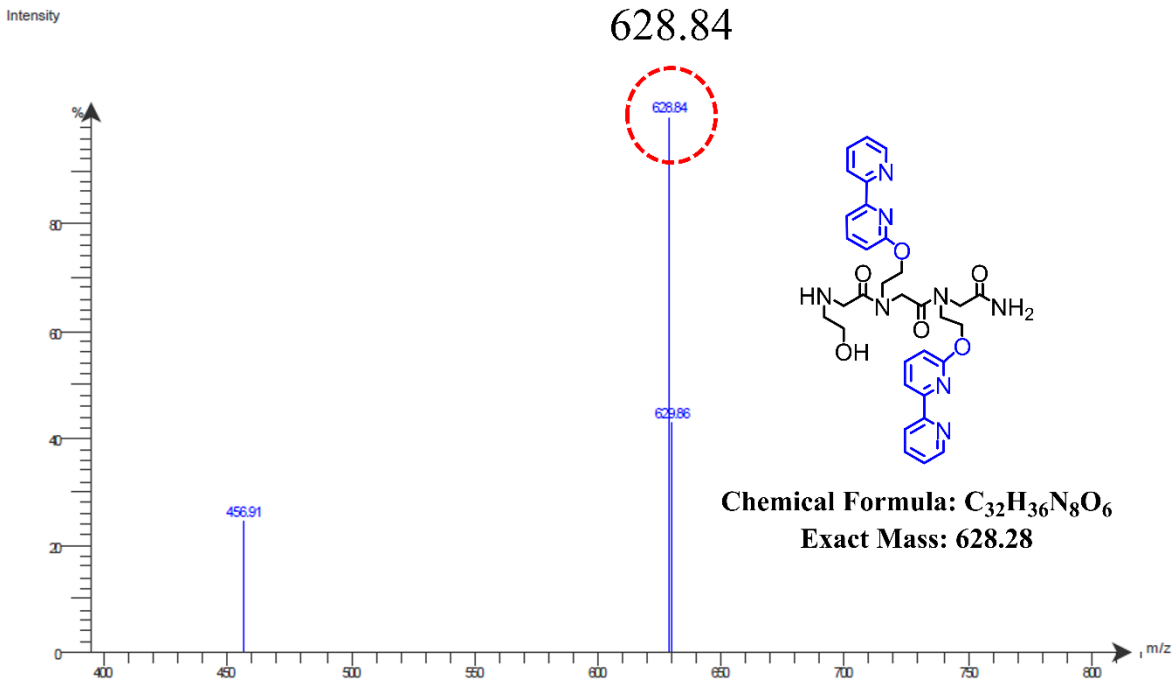

Figure S19. ESI-MS of peptoid **BBE**.

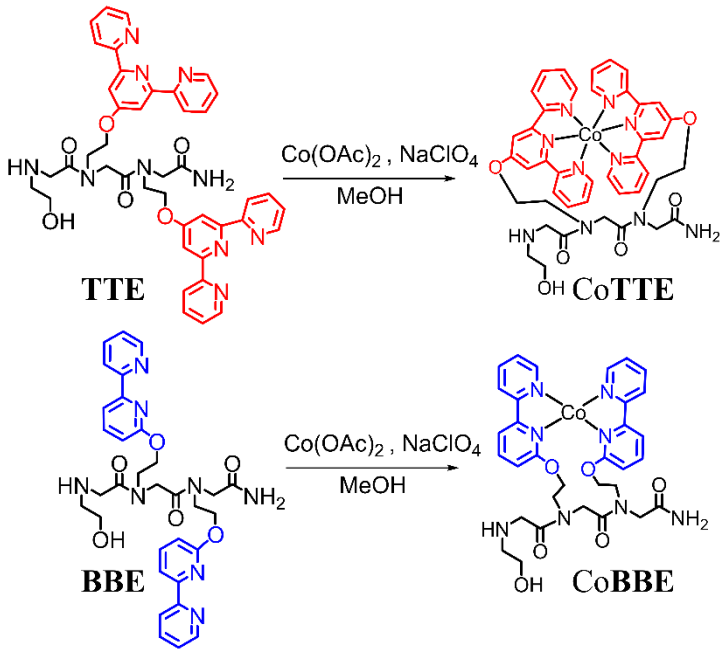

Scheme S1. The molecular structures of peptoid **TTE, BBE** and corresponding Co complexes Co**TTE** and Co**BBE** with the same complexation method as Co**TBE.**

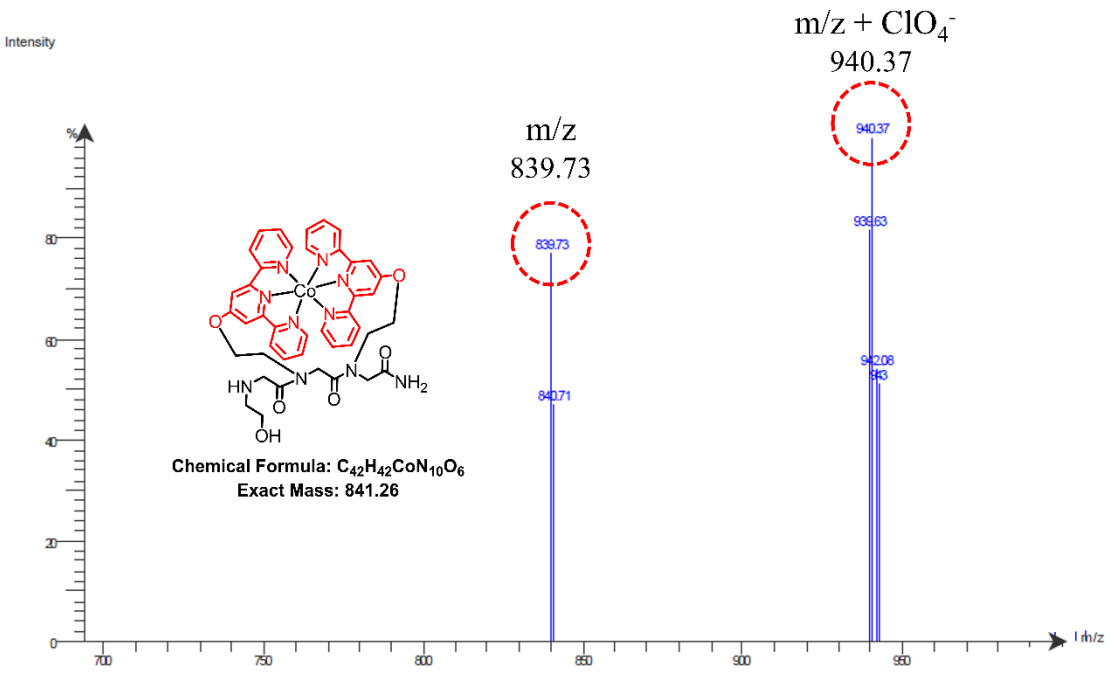

Figure S20. ESI-MS of peptoid Co**TTB**.

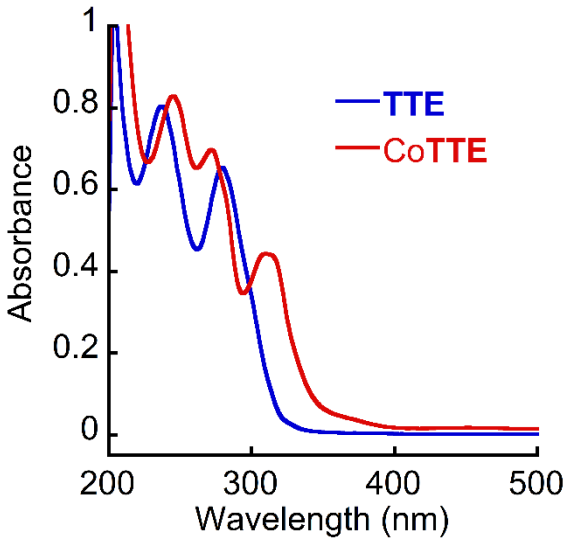

Figure S21. UV-Vis spectra of ~25 µM of the peptoid **TTE** and complex Co**TTE** in PBS at pH7.

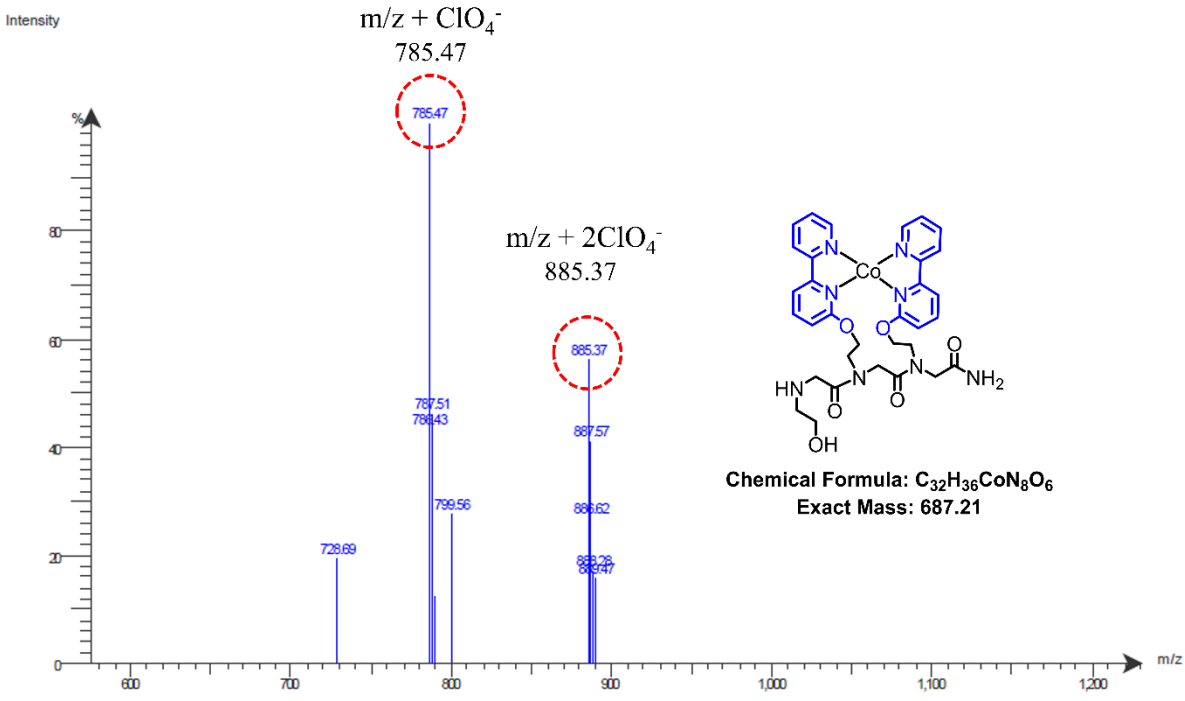

Figure S22. ESI-MS of peptoid Co**TTB**.

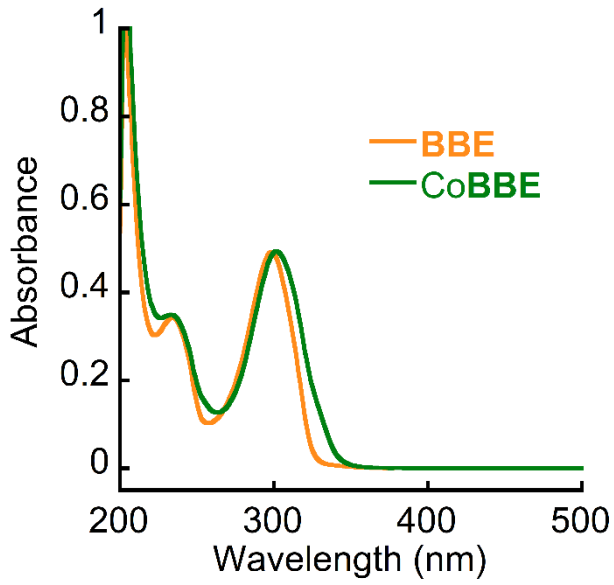

Figure S23. UV-Vis spectra of ~25 µM of the peptoid **BBE** and complex Co**BBE** in PBS at pH7.

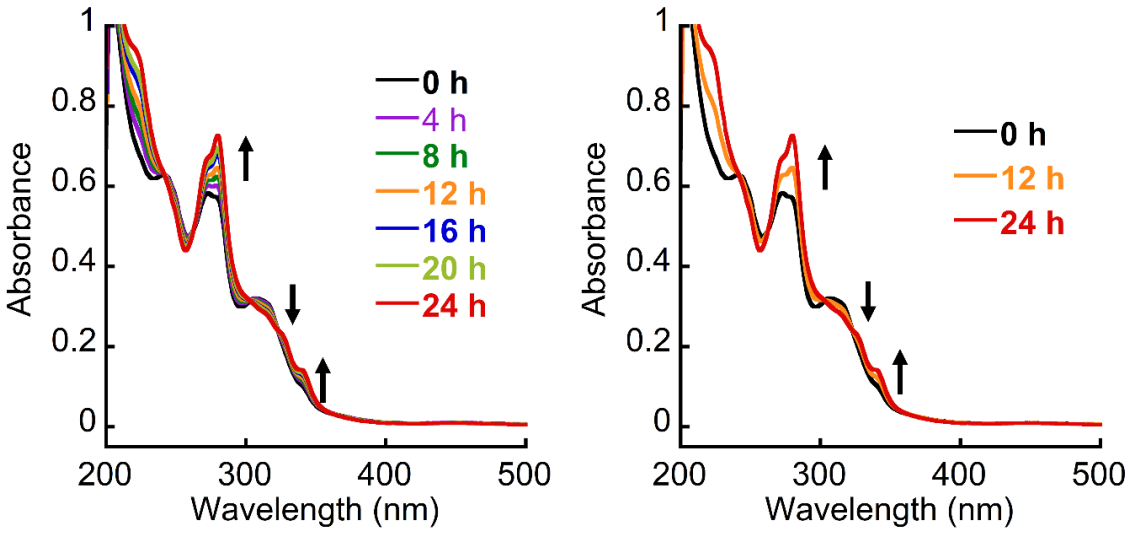

Figure S24. UV-Vis absorption spectra of Co**TTE** in 0.1M phosphate buffer at pH 7 without disturbing for 24 hours.

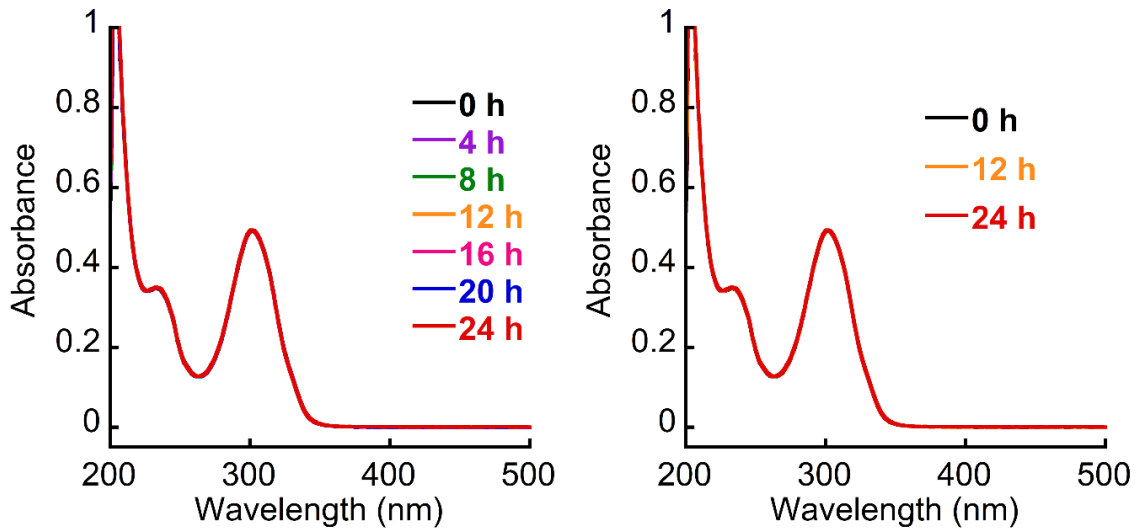

Figure S25. UV-Vis absorption spectra of Co**BBE** in 0.1M phosphate buffer at pH 7 without disturbing for 24 hours.

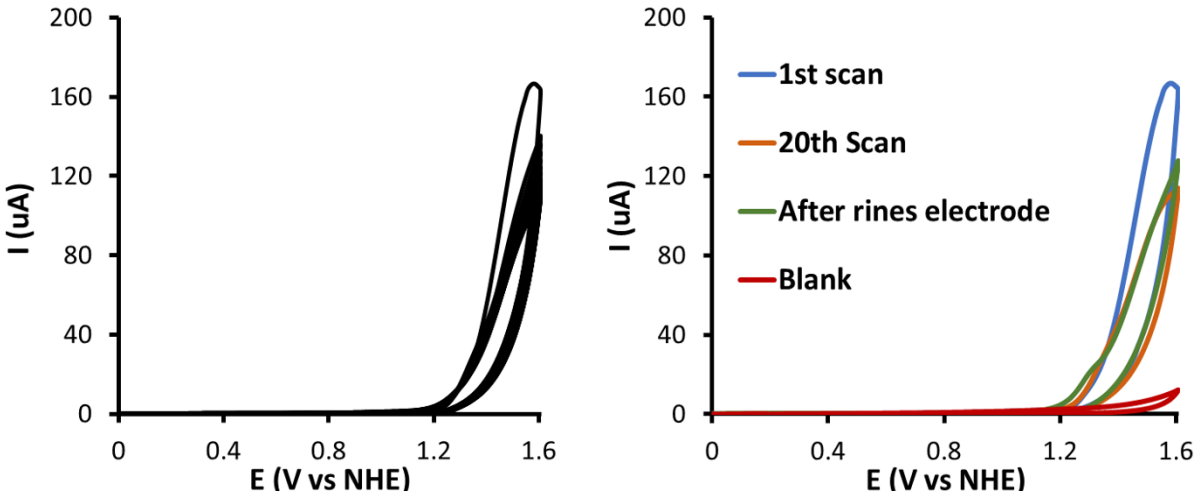

Figure S26. Continuous 20 CVs of 0.5 mM Co**BBE** at scan rate 100 mV/s in 0.1 M phosphate buffer solution at pH 7.

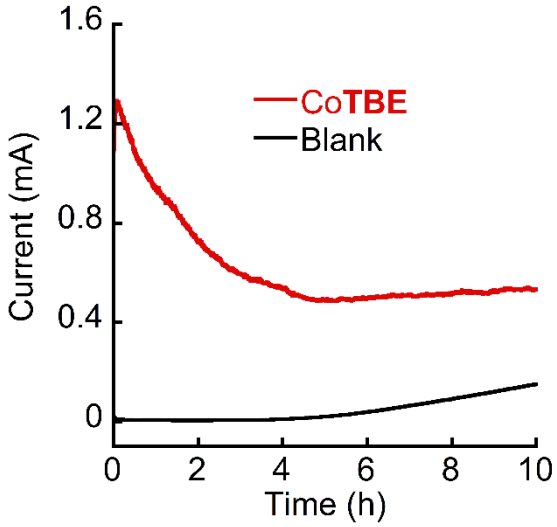

Figure S27. Total current passed during control potential electrolysis hours in 0.1 M phosphate buffer at pH 7.0 containing 0.5 mM catalyst Co**TBE** and the buffer only using a porous glassy carbon at +1.25 V vs. NHE for 10 hours.

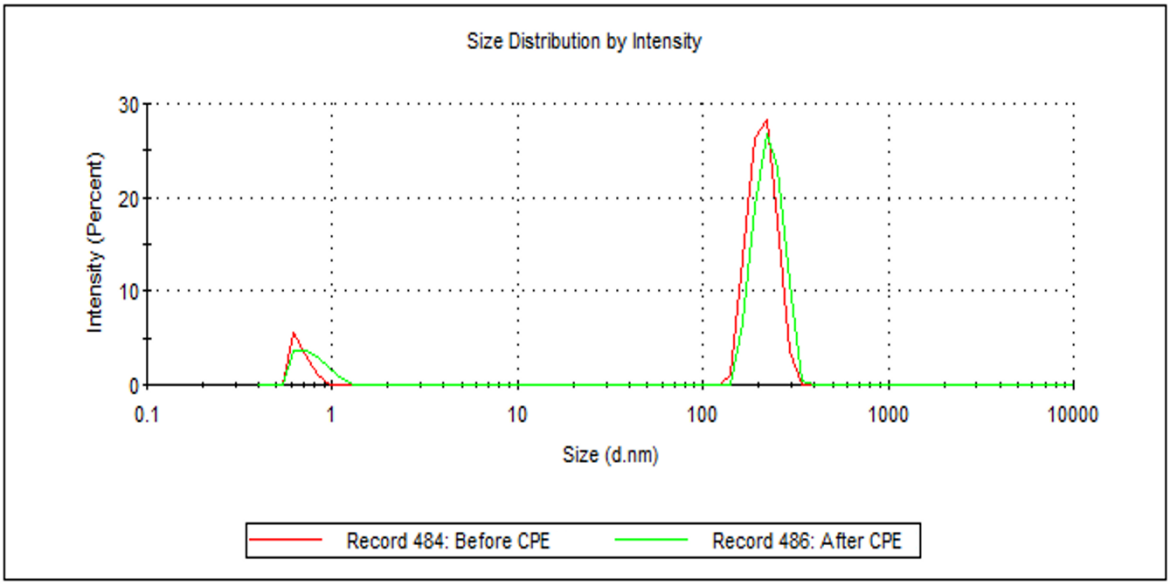

Figure S28. DLS spectra of Co**TBE** solution before (red spectra) and after (green spectra) CPE.

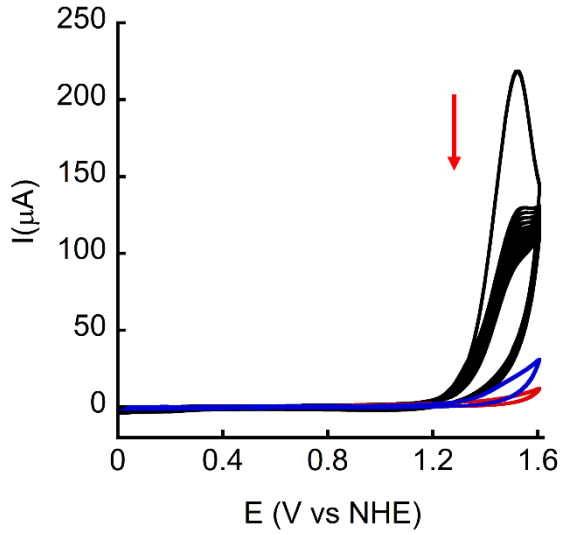

Figure S29. Continuous 20 CVs of 0.5 mM Co**TBE** (black), buffer solution without catalyst (red) and blank buffer solution after rinse the electrode with water without polishing (blue). All CVs were measured at scan rate 100 mV/s in 0.1 M phosphate buffer solution at pH 7.

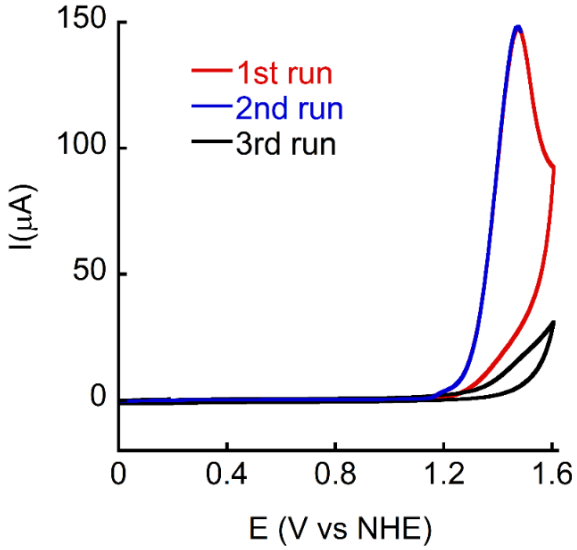

Figure S30. The rinse test of the complex Co**TBE** was performed to find out the nature of the catalyst, i.e., whether it is heterogeneous or homogeneous. To prove that we have performed three consecutive cv runs (scan rate 20 mV/s). In the first run, a complete scan was recorded for the complex in PBS pH 7 (red line). Then, the working electrode was thoroughly rinsed with water and polished to remove any possible heterogeneous species formed on the electrode surface. Afterward, a second run was performed in the same solution containing the complexes with the cleaned electrode. Here, this second run was stopped at a positive potential, close to the potential where the maximum catalytic current was observed (blue line). Then, the working electrode was only rinsed with water (not polished) and a third run was recorded in a fresh catalyst free buffer solution (black line). Here as the third run did not exhibit any catalytic current compared to the first two runs, it concluded that the catalytic current is generated due to homogeneous catalytic pathway.[5]

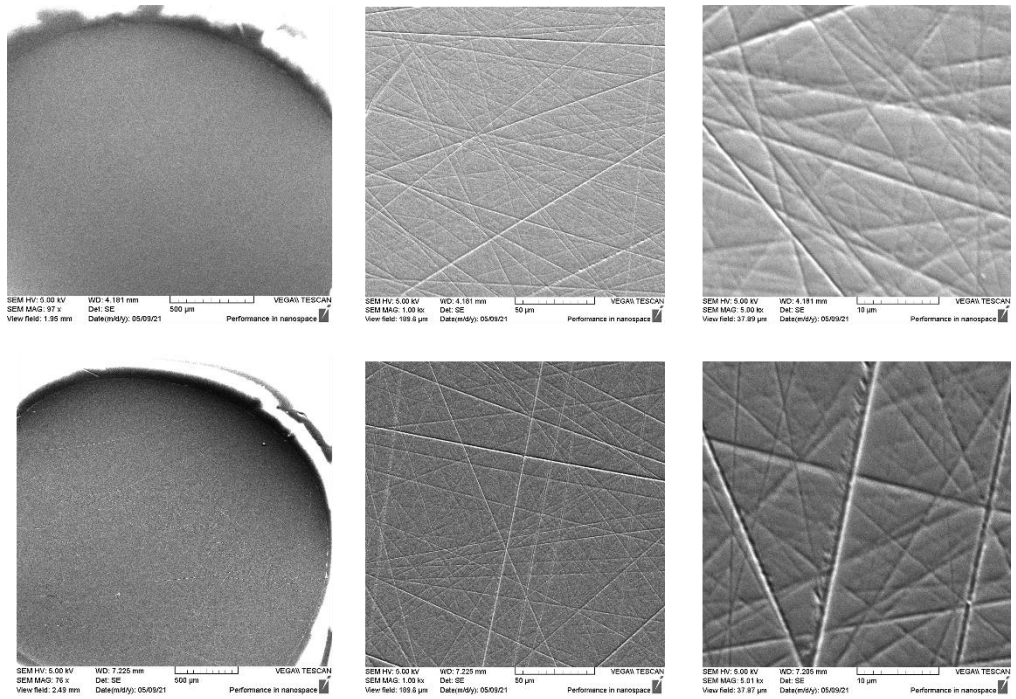

Figure S31. SEM images of the glassy carbon electrode before (up) and after (down) continuous 20 CV scans measured in different scales.

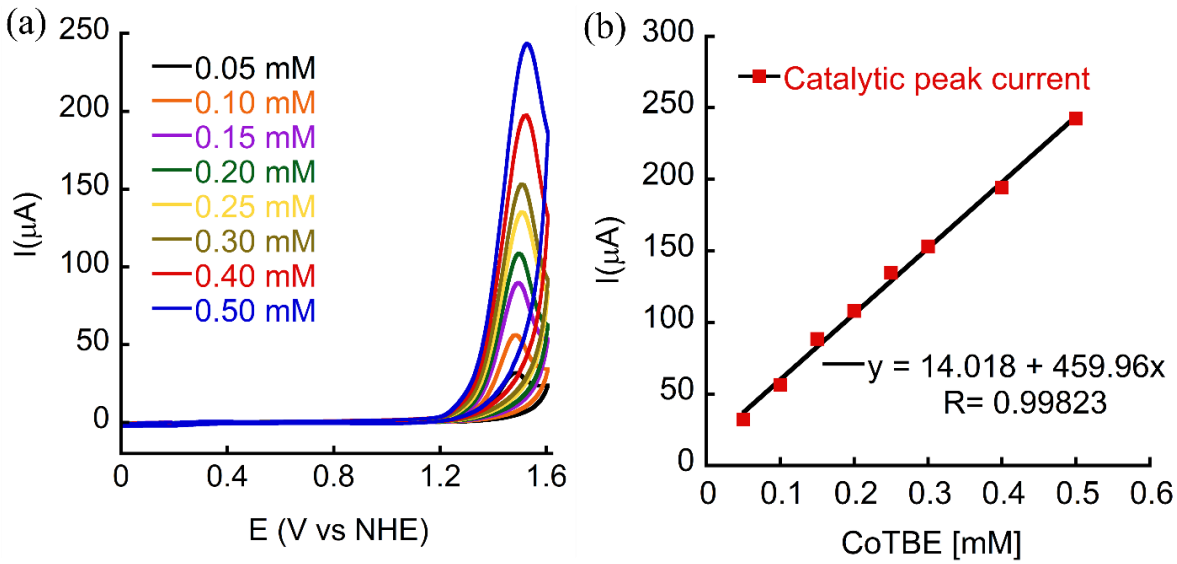

Figure S32. (a) CVs of Co**TBE** having different concentration in 0.1 M PBS at pH 7. (b) Linear regression of i_{cat} versus different concentration of Co**TBE**.

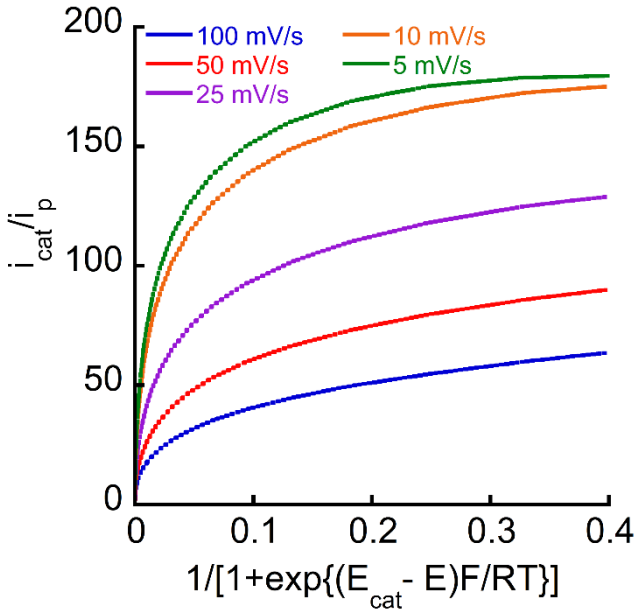

Figure S33. FOWA plotting i_{cat}/i_p v. 1/(1+exp[(E_{cat} - E)F/RT]) at each scan rate. The averaged kobs of catalyst Co(T**BE**), 5.76 x 10^4 s^{-1}, obtained from the mean of (4.11, 5.06, 7.18, 7.75, 4.71) x 10^4 s^{-1} at scan rates 100, 50, 25, 10, 5 mV/s, respectively.

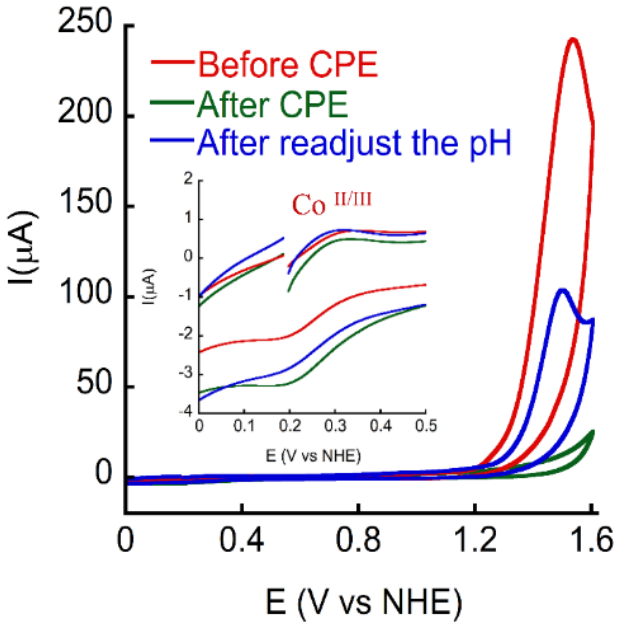

Figure S34. CVs of 0.5mM Co**TBE** in 0.1M phosphate buffer solution at pH = 7.0 before and after 10-hours CPE experiment with +1.25 V applied potential and after readjusting the pH back to 7 (scan rate =100 mV/s).

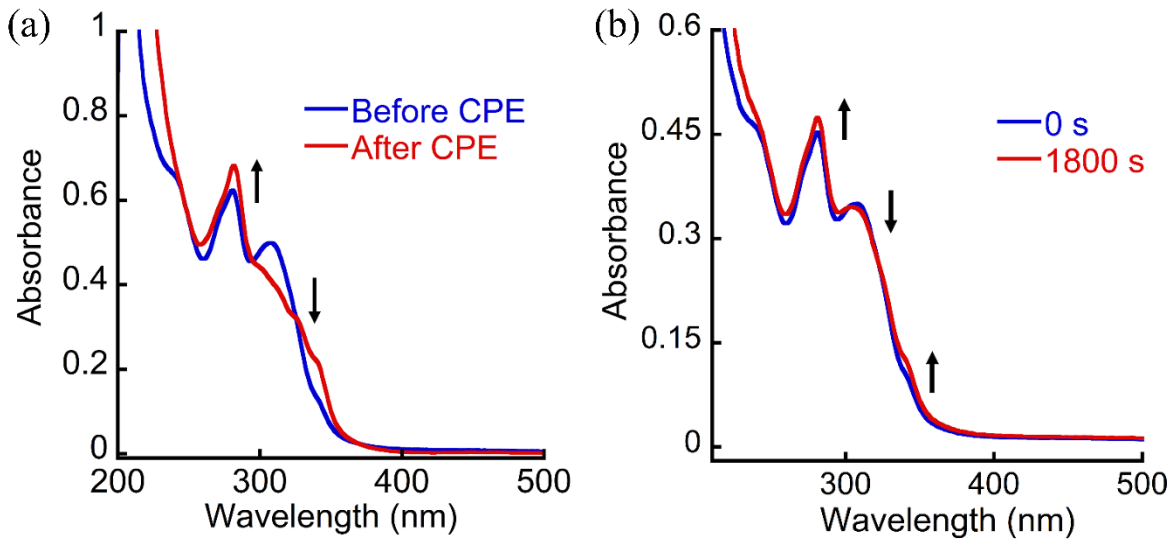

Figure S35. (a) UV-Vis absorption spectra of ~25 µM of Co**TBE** before and after 10 hours CPE experiments +1.25 V applied potential in 0.1M phosphate buffer at pH 7, (b) UV−vis spectroscopy of ~20 µM Co**TBE** during spectroelectrochemistry experiment at an applied potential of 1.53 V in 0.1 M phosphate buffer at pH 7.

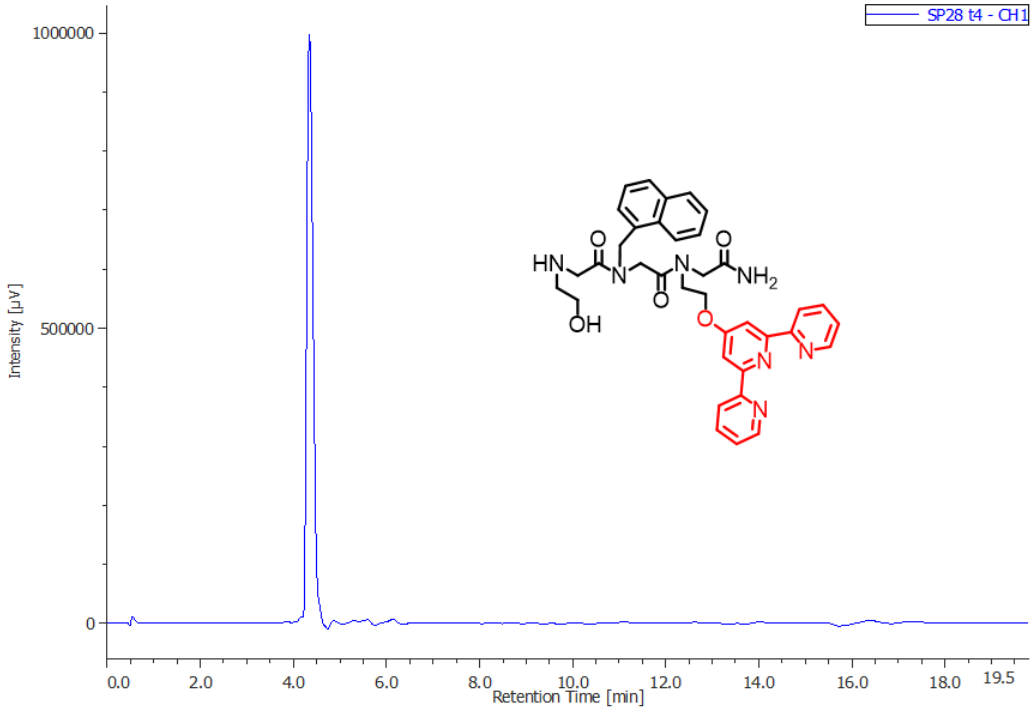

Figure S36. HPLC traces of pure peptoid **TE.**

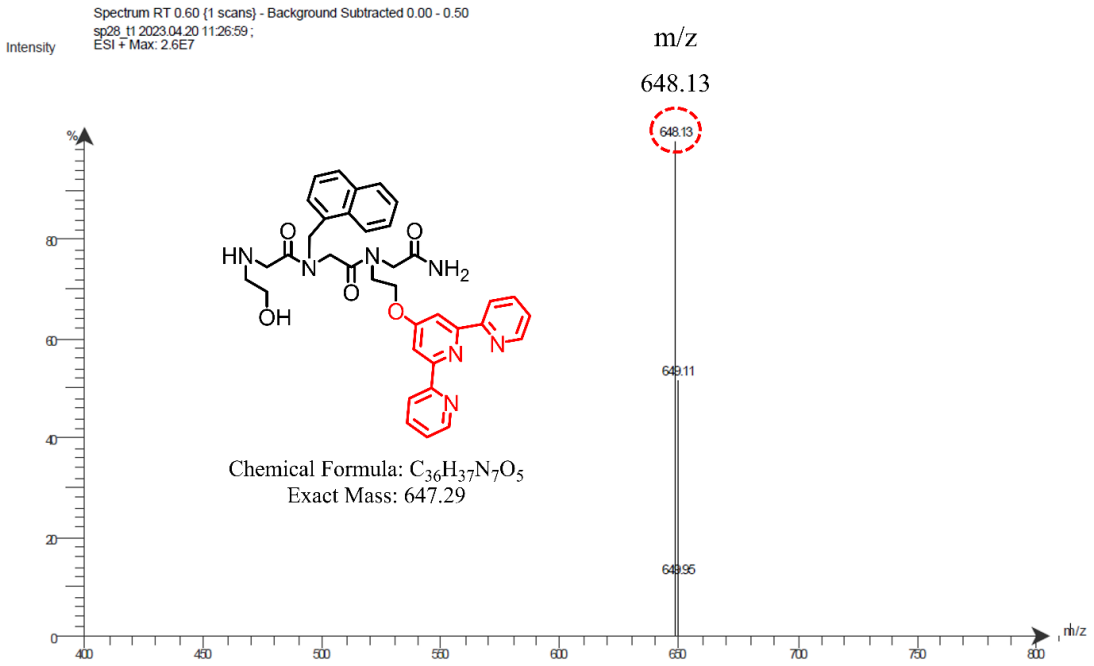

Figure S37. ESI-MS of peptoid **TE.**

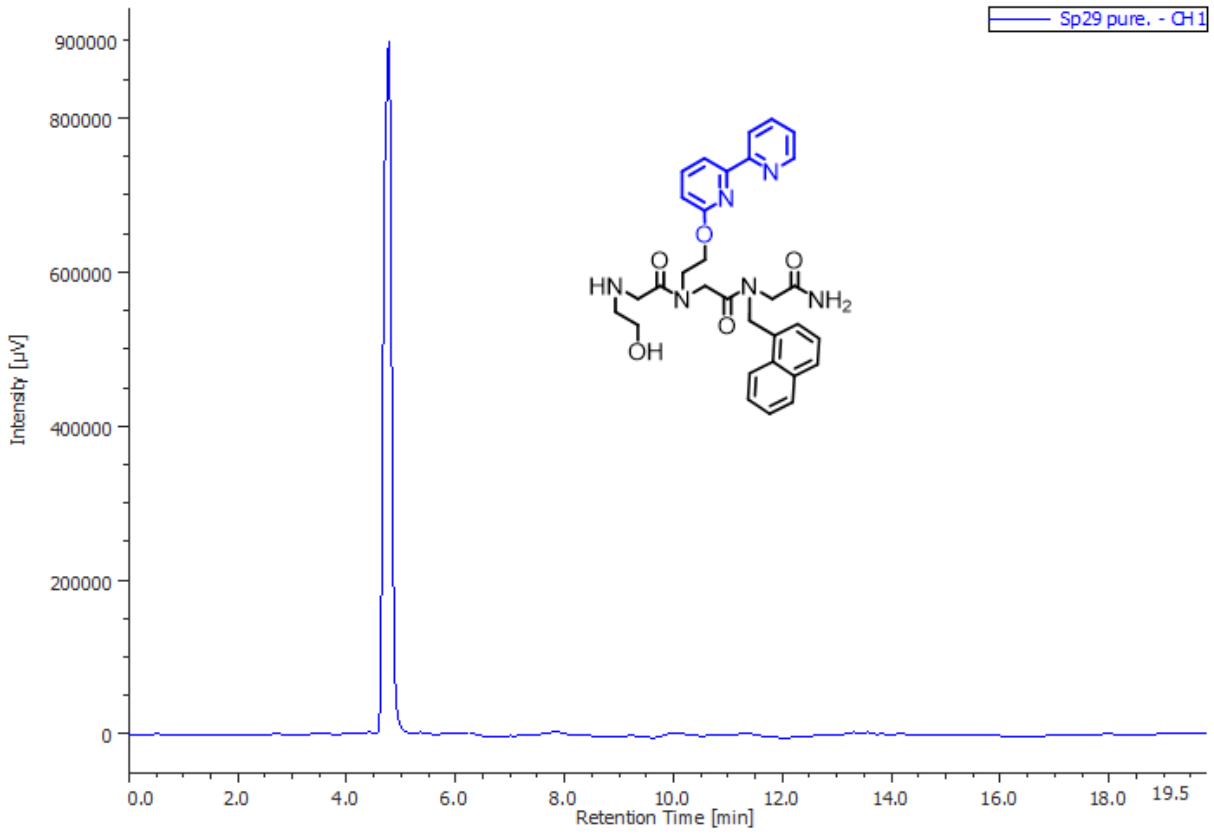

Figure S38. HPLC traces of pure peptoid **BE.**

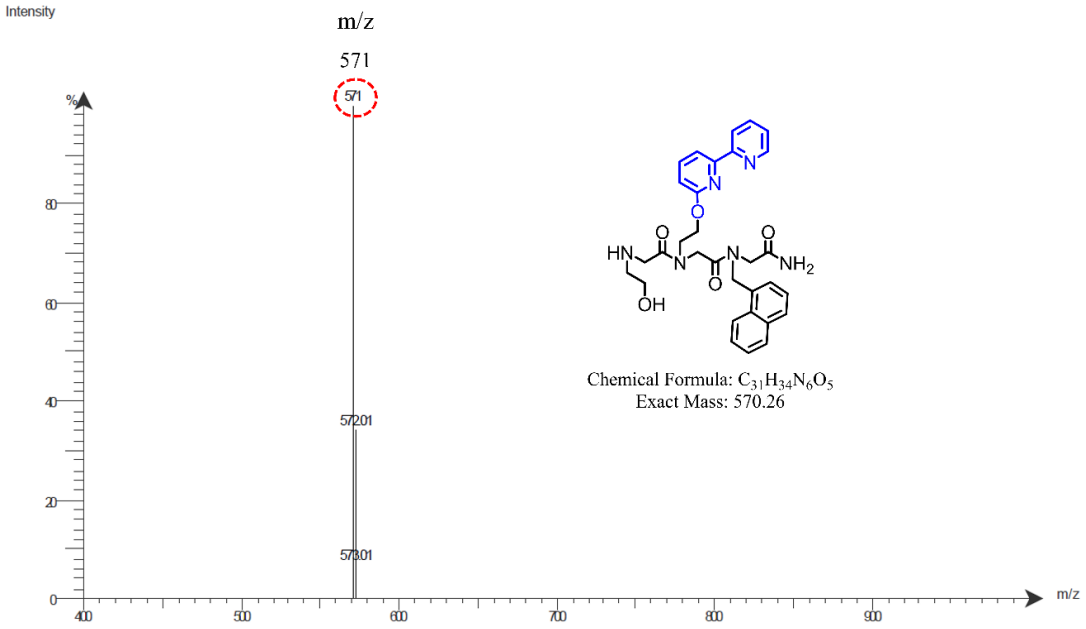

Figure S39. ESI-MS of peptoid **BE.**

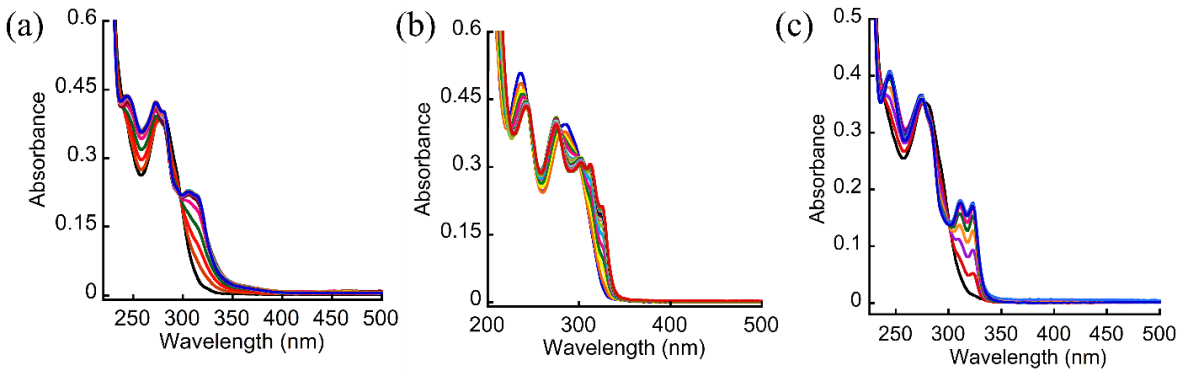

Figure S40. UV-Vis titration spectra of **TE** (20 μM) with (a) Co, (b) Ni and (c) Zn in 0.1 M phosphate buffer at pH 7 up to 2 equivalent.

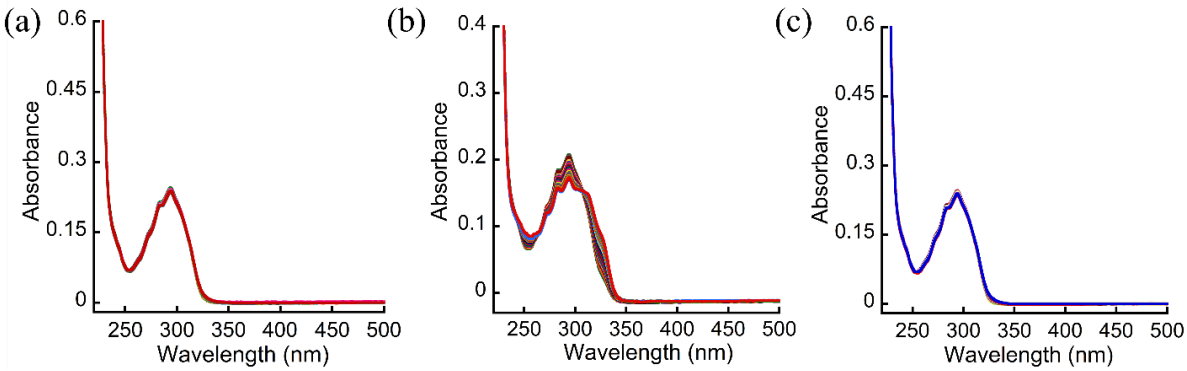

Figure S41. UV-Vis titration spectra of **BE** (20 μM) with (a) Co, (b) Ni and (c) Zn in 0.1 M phosphate buffer at pH 7 up to 2 equivalent.

Peptoid	UV-Vis titration with Co	UV-Vis titration with Ni	UV-Vis titration with Zn
TE	**314 nm**	**313 nm, 326 nm**	**311 nm, 323 nm**
BE	**-**	**315 nm, 329 nm**	**-**

Table S1. Binding properties of **TB** and **TE** from their UV–Vis titration with Co, Ni and Zn in phosphate buffer at pH7.

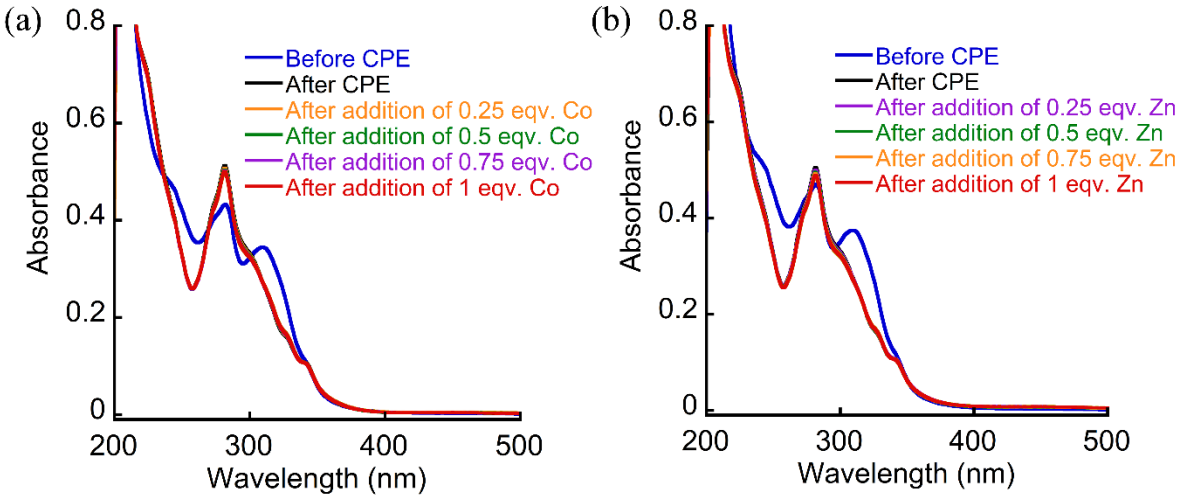

Figure S42. UV-Vis titration spectra of dried sample after CPE with (a) Co and (b) Zn in 0.1M phosphate buffer solution at pH = 7.0.

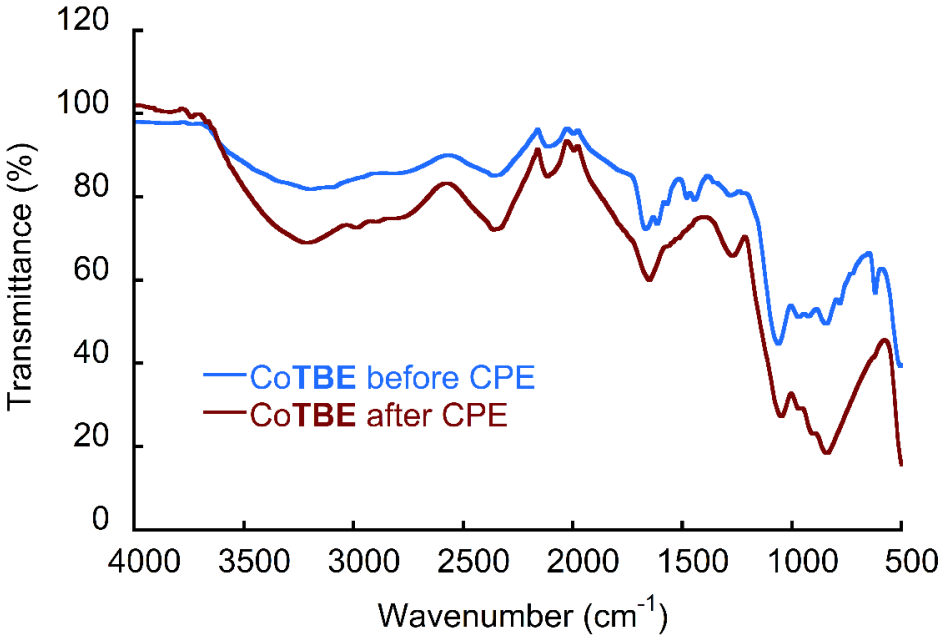

Figure S43. FTIR of the dried solid complex Co**TBE** before and after a 10-hour CPE experiment with +1.25 V applied potential in 0.1 M phosphate buffer at pH 7.

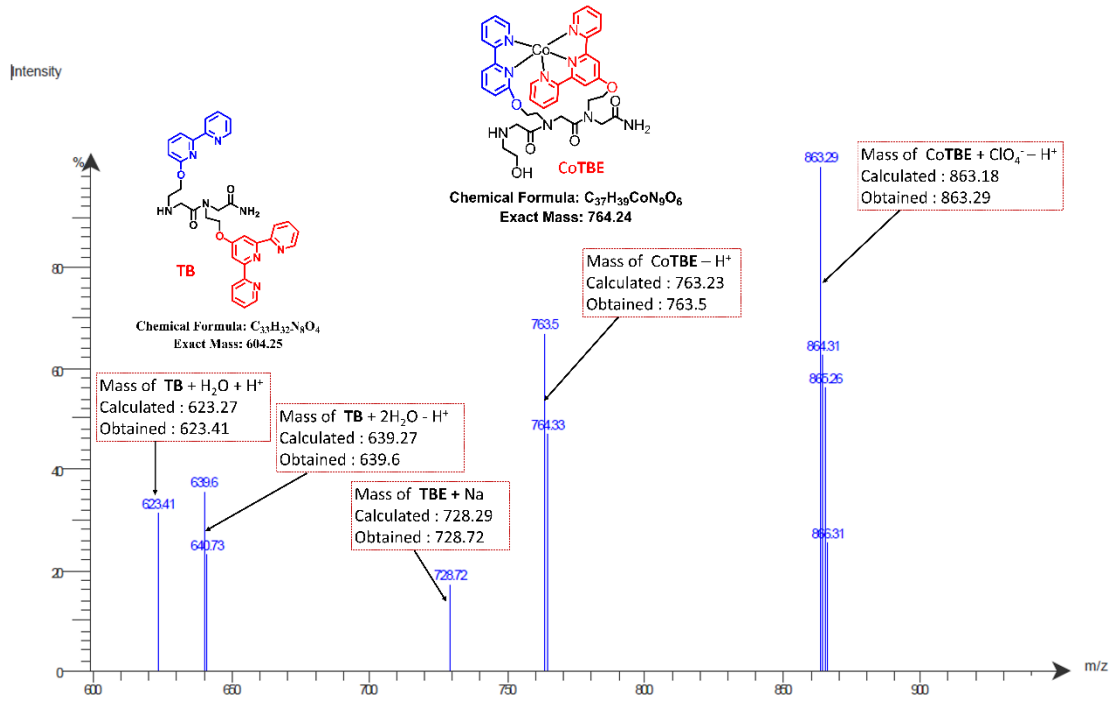

Figure S44. ESI-MS of the catalytic solution of Co**TBE** before CPE in 0.1M phosphate buffer solution at pH = 7.0.

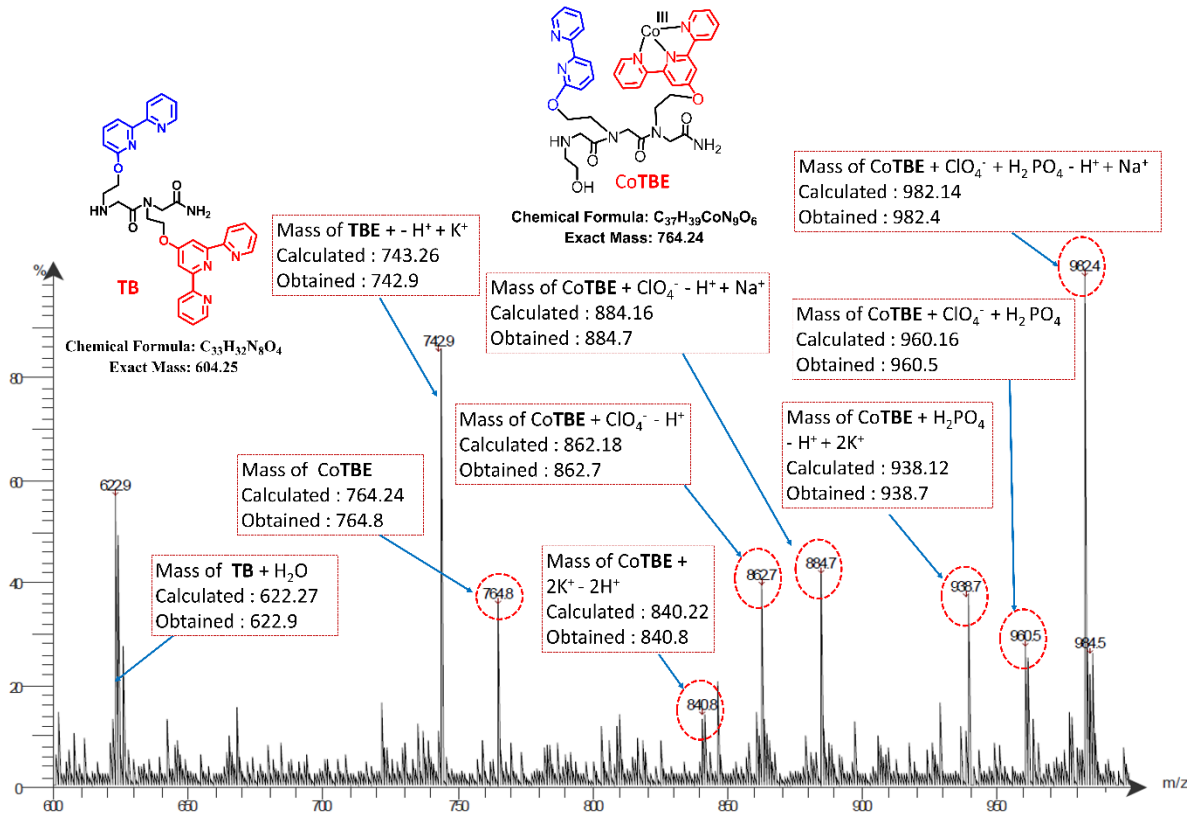

Figure S45. ESI-MS of the catalytic solution of Co**TBE** after 10 hours CPE at 1.25 V vs NHE in 0.1M phosphate buffer solution at pH = 7.0.

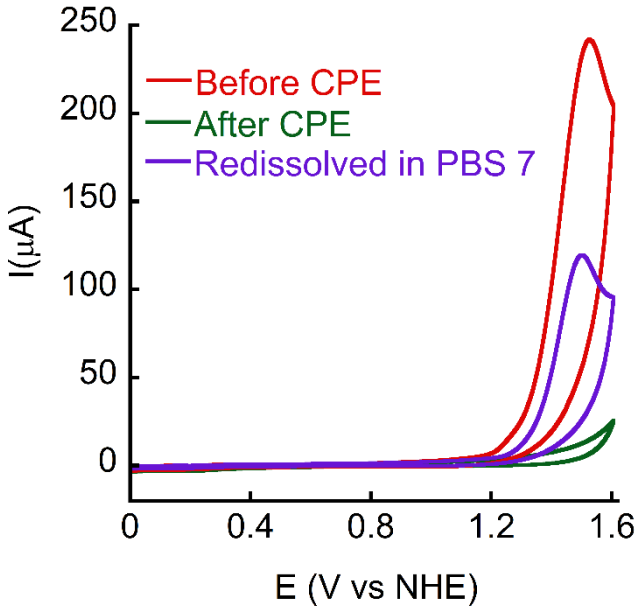

Figure S46. CVs of 0.5mM Co**TBE** in 0.1M phosphate buffer solution at pH = 7.0 before, after 10-hours CPE experiment with +1.25 V applied potential and after redissolved the isolated CPE solution in PBS at pH 7 (scan rate =100 mV/s).

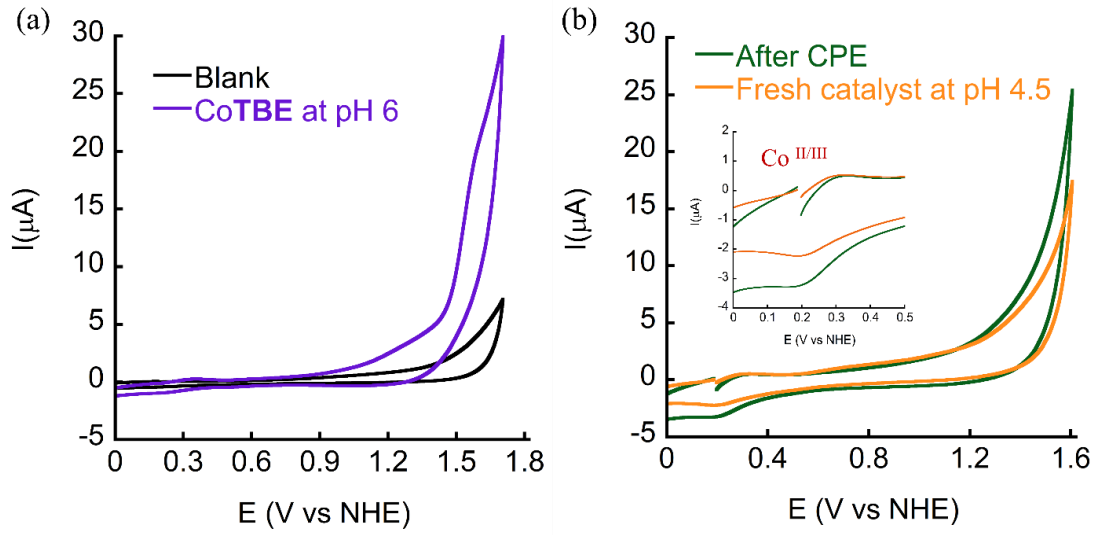

Figure S47. (a) CV of fresh complex Co**TBE** in 0.1M phosphate buffer solution at pH = 6, (b) CV of fresh complex Co**TBE** in 0.1M phosphate buffer solution at pH = 4.5 and CV after 10 hours CPE with +1.25 V applied potential (scan rate =100 mV/s).

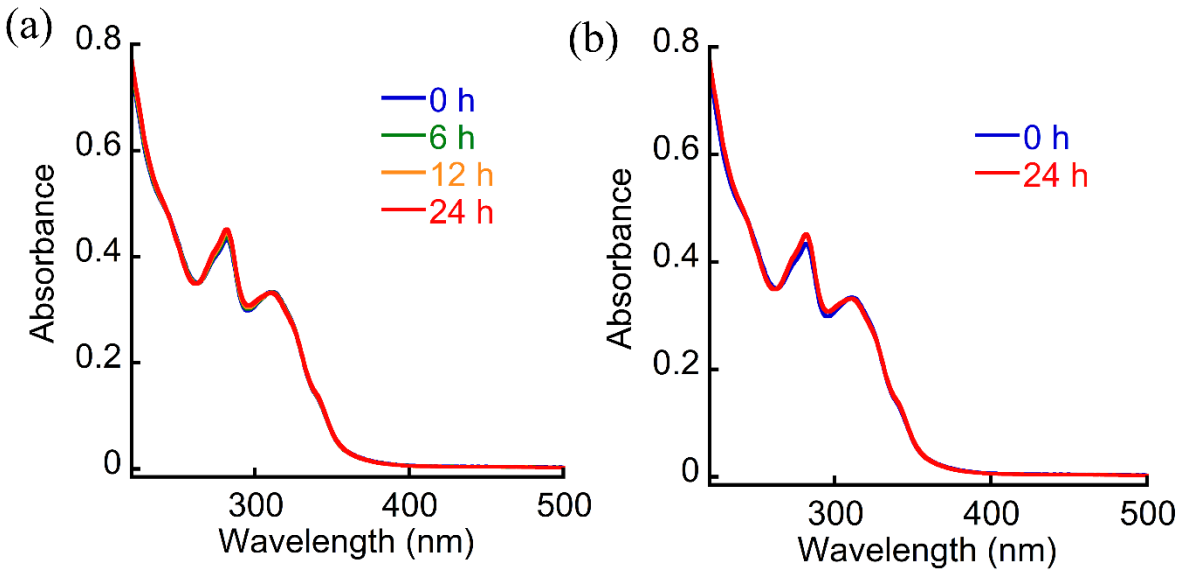

Figure S48. UV-Vis absorption spectra of Co**TBE** in 0.1M phosphate buffer at pH 6 without disturbing for 24 hours.

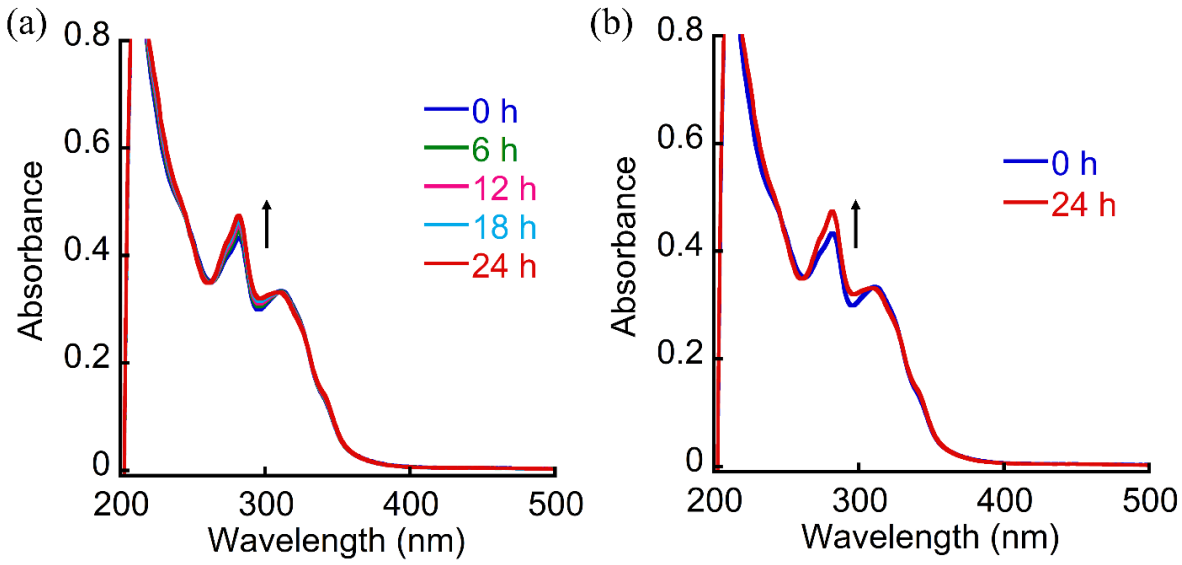

Figure S49. UV-Vis absorption spectra of Co**TBE** in 0.1M phosphate buffer at pH 4.5 without disturbing for 24 hours.

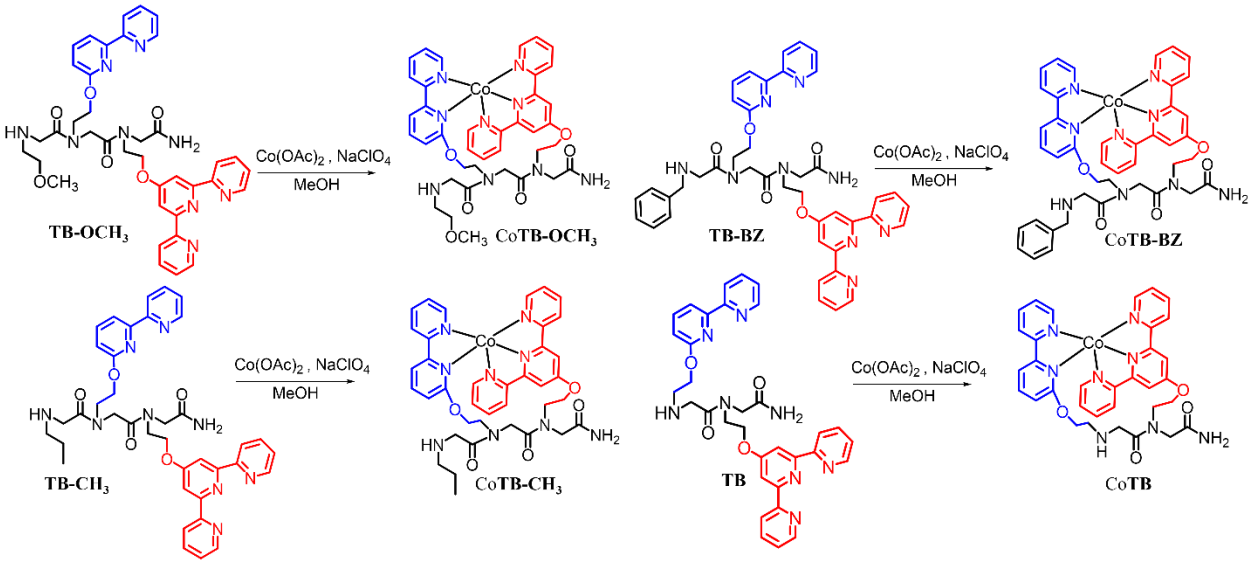

Scheme S2. The molecular structures of peptoid **TB-OCH3, TB-CH3, TB-BZ, TB** and corresponding Co complexes Co**TB-OCH3**, Co**TB-CH3**, Co**TB-BZ** and Co**TB** with the same complexation method as Co**TBE**.

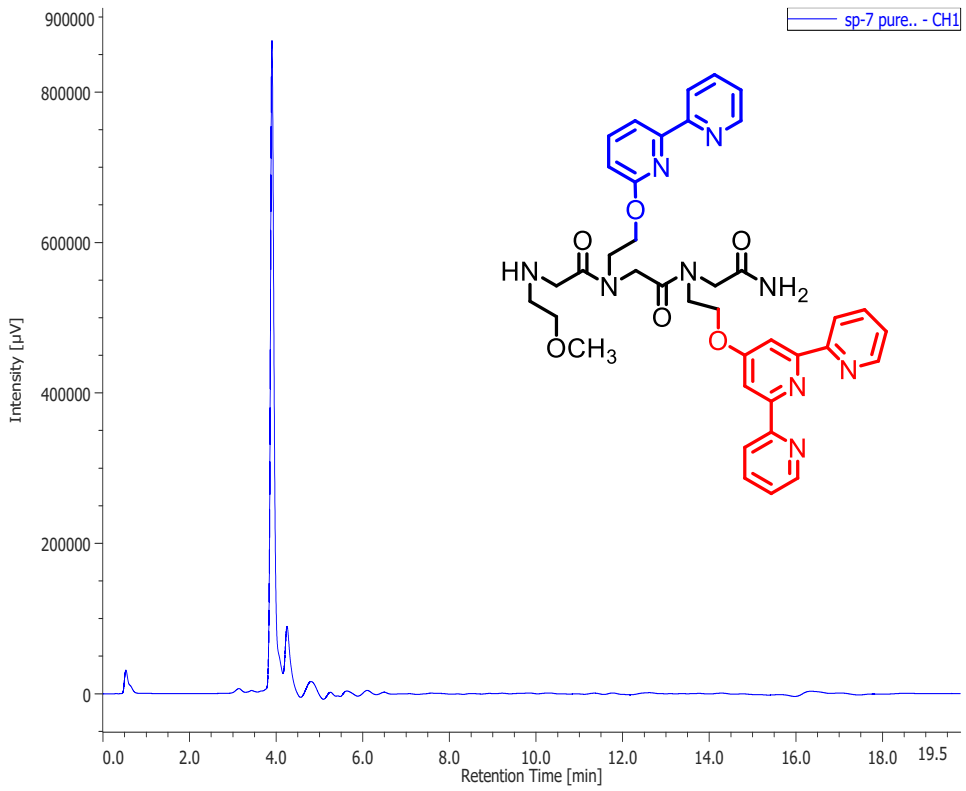

Figure S50. HPLC traces of pure peptoid **TB-OCH3**

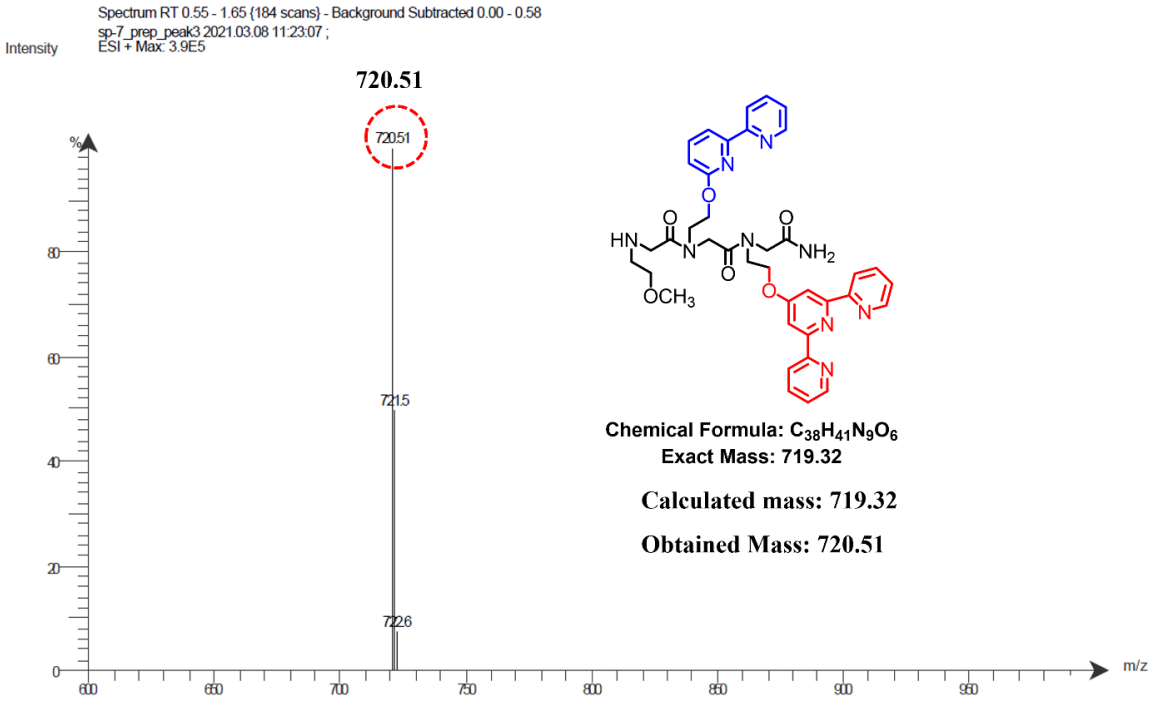

Figure S51. ESI-MS of peptoid **TB-OCH3**

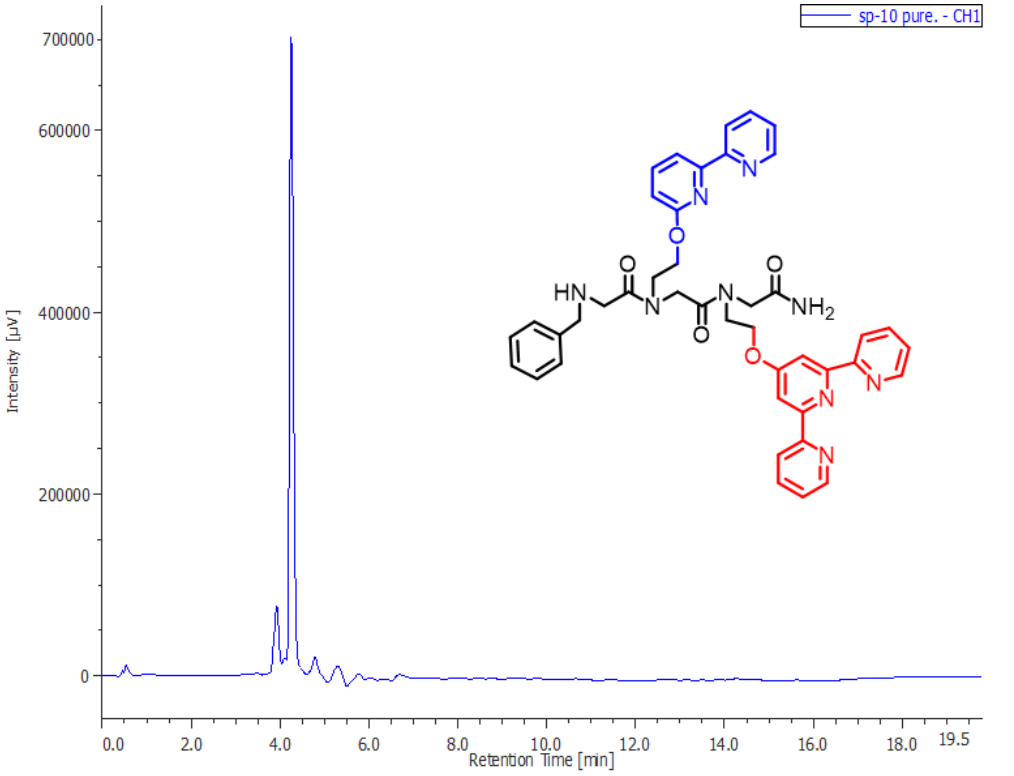

Figure S52. HPLC traces of pure peptoid **TB-BZ**

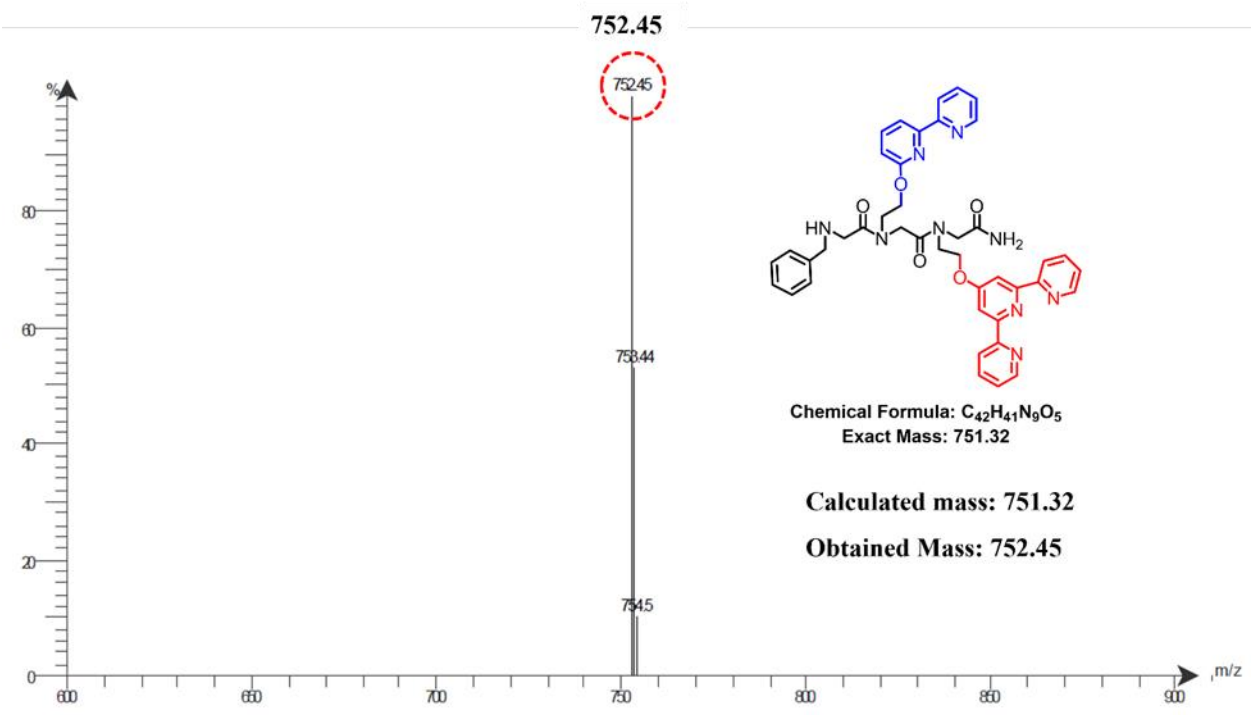

Figure S53. ESI-MS of peptoid **TB-BZ**

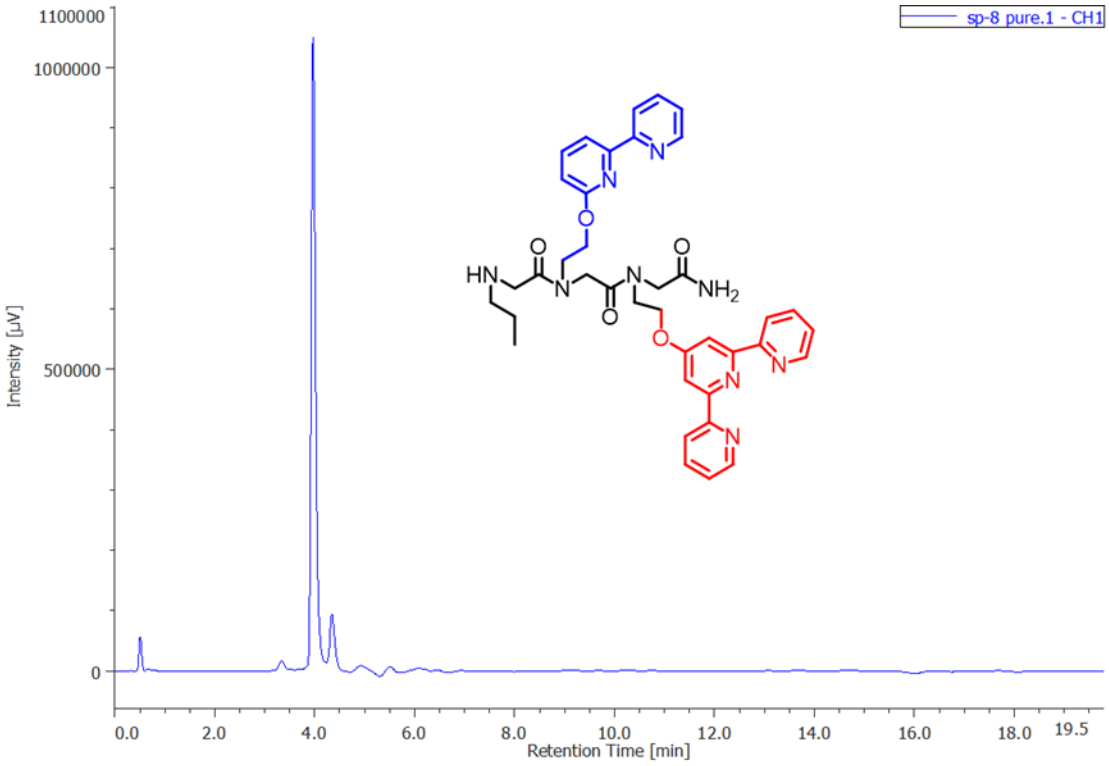

Figure S54. HPLC traces of pure peptoid **TB-CH$_3$**

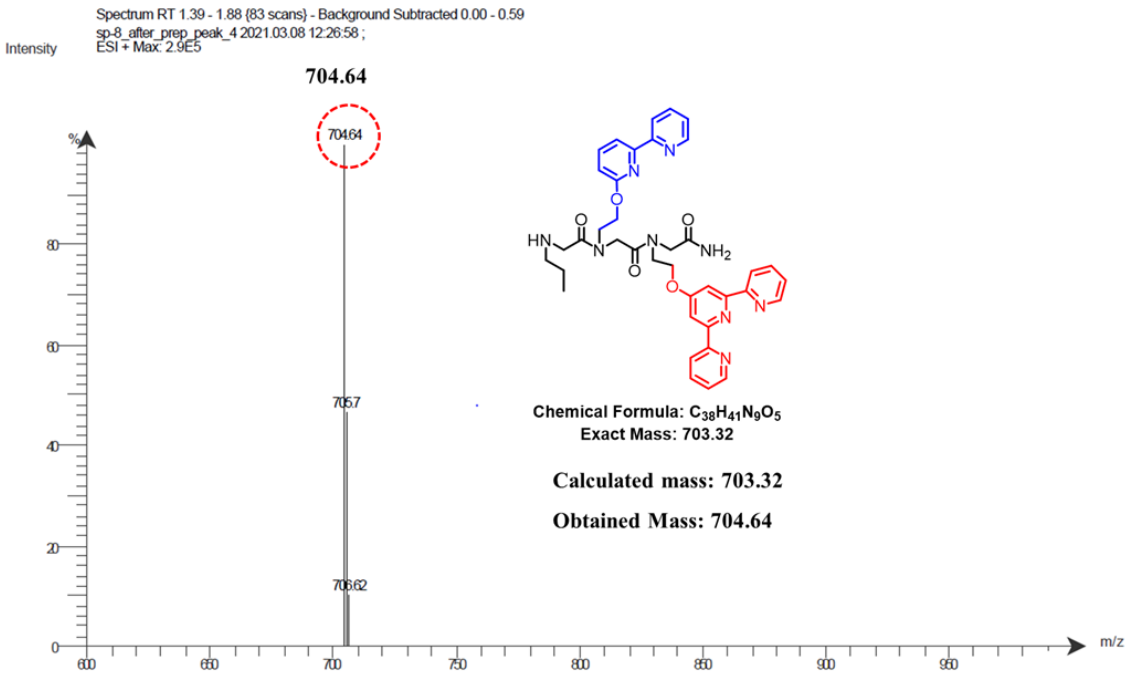

Figure S55. ESI-MS of peptoid **TB-CH$_3$**

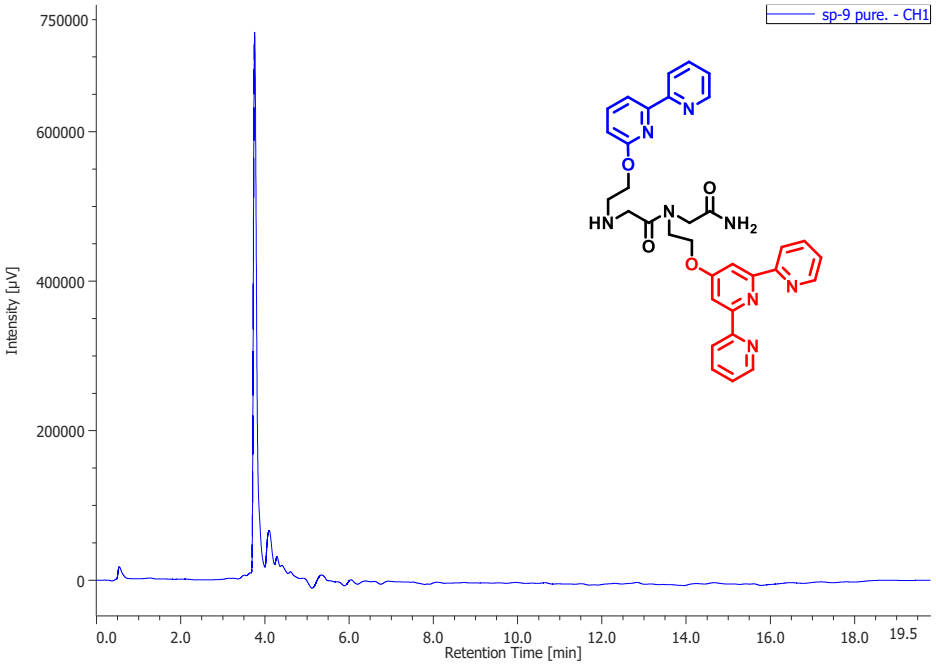

Figure S56. HPLC traces of pure peptoid **TB**

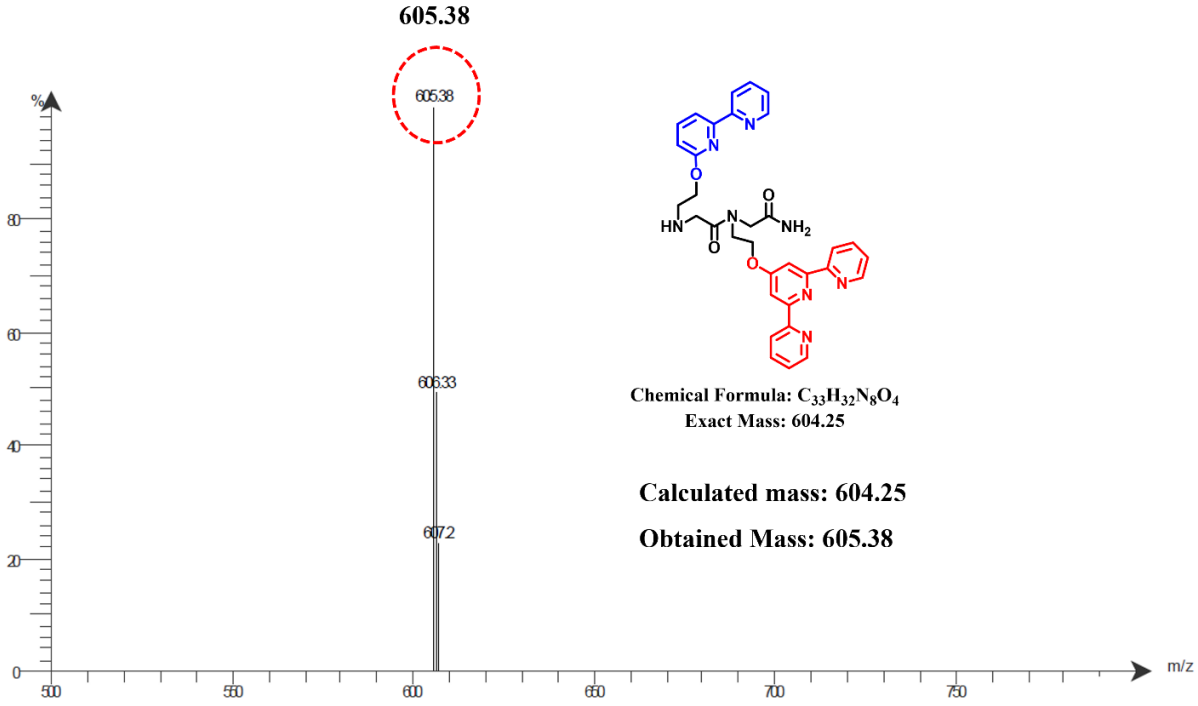

Figure S57. ESI-MS of peptoid **TB**

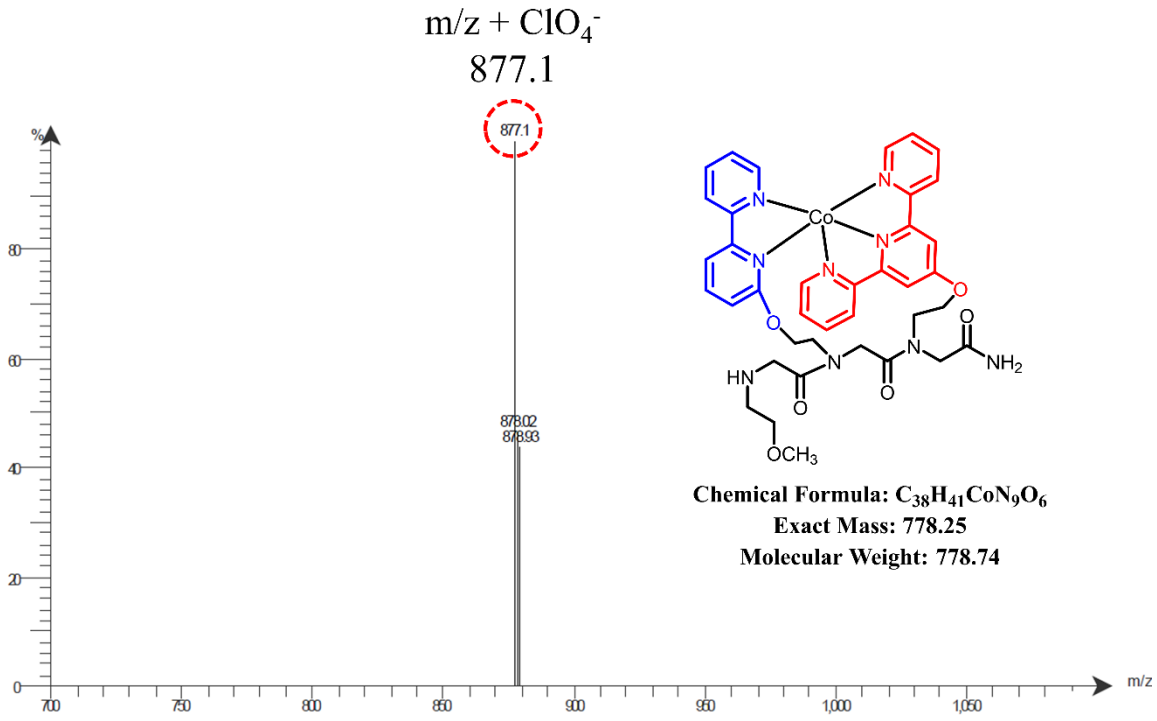

Figure S58. ESI-MS of peptoid Co**TB-OCH3**

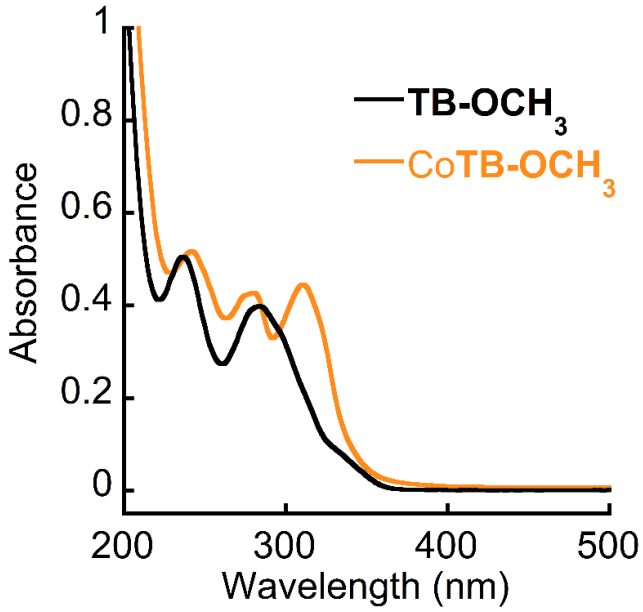

Figure S59. UV-Vis spectra of 25 µM of the peptoid **TB-OCH3** and complex Co**TB-OCH3** in PBS at pH 7.

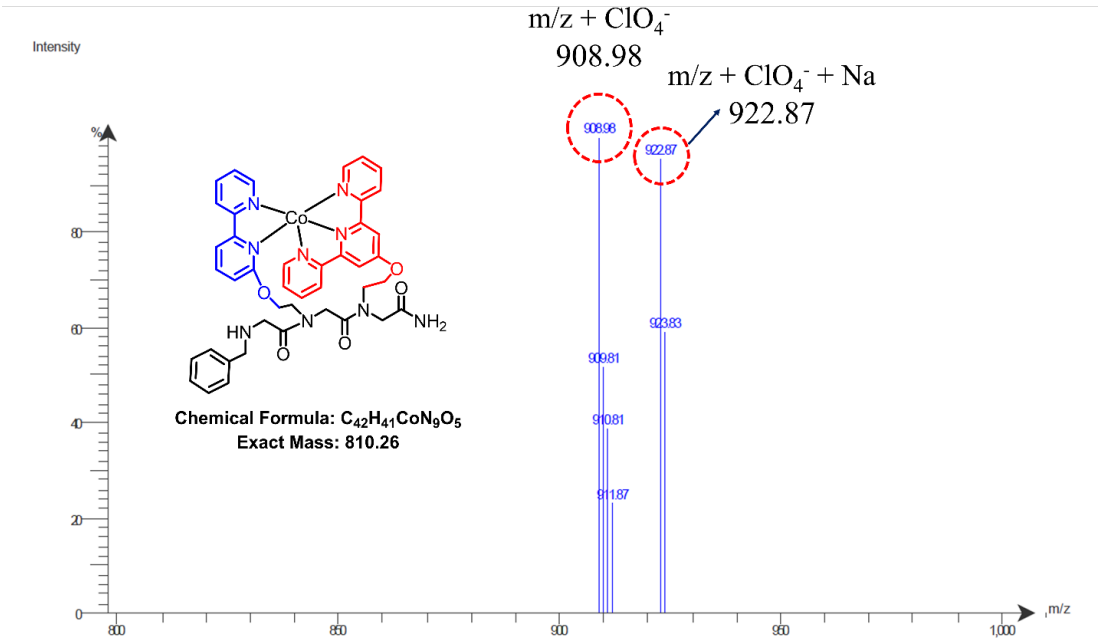

Figure S60. ESI-MS of peptoid Co**TB-BZ**.

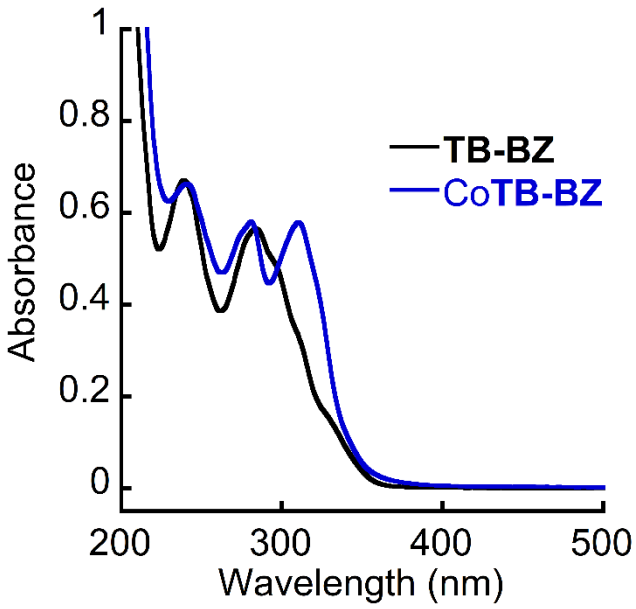

Figure S61. UV-Vis spectra of 25 µM of the peptoid **TB-BZ** and complex Co**TB-BZ** in PBS at pH 7.

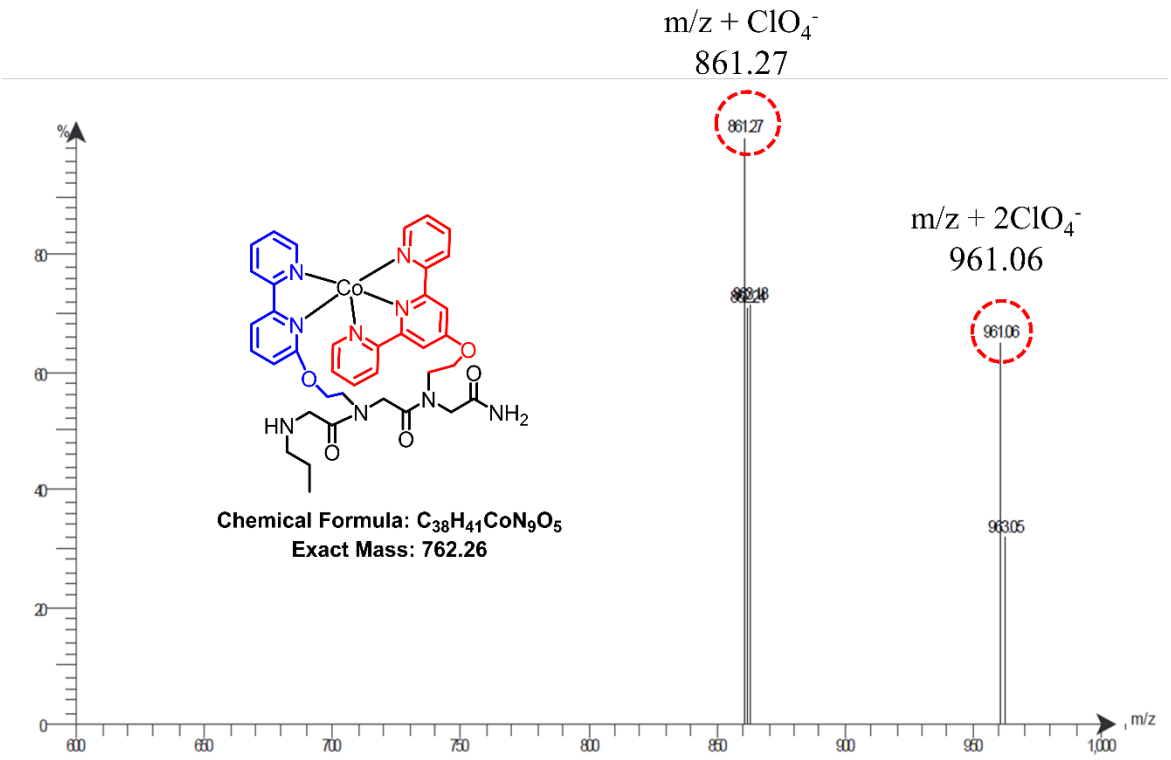

Figure S62. ESI-MS of peptoid Co**TB-CH3**.

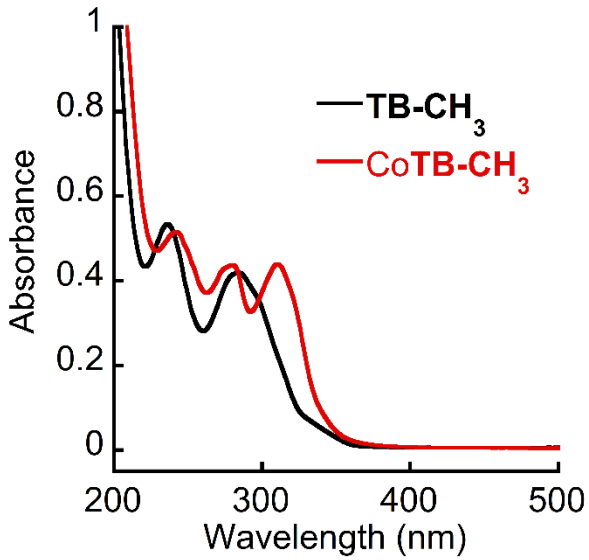

Figure S63. UV-Vis spectra of 25 µM of the peptoid **TB-CH3** and complex Co**TB-CH3** in PBS pH 7.

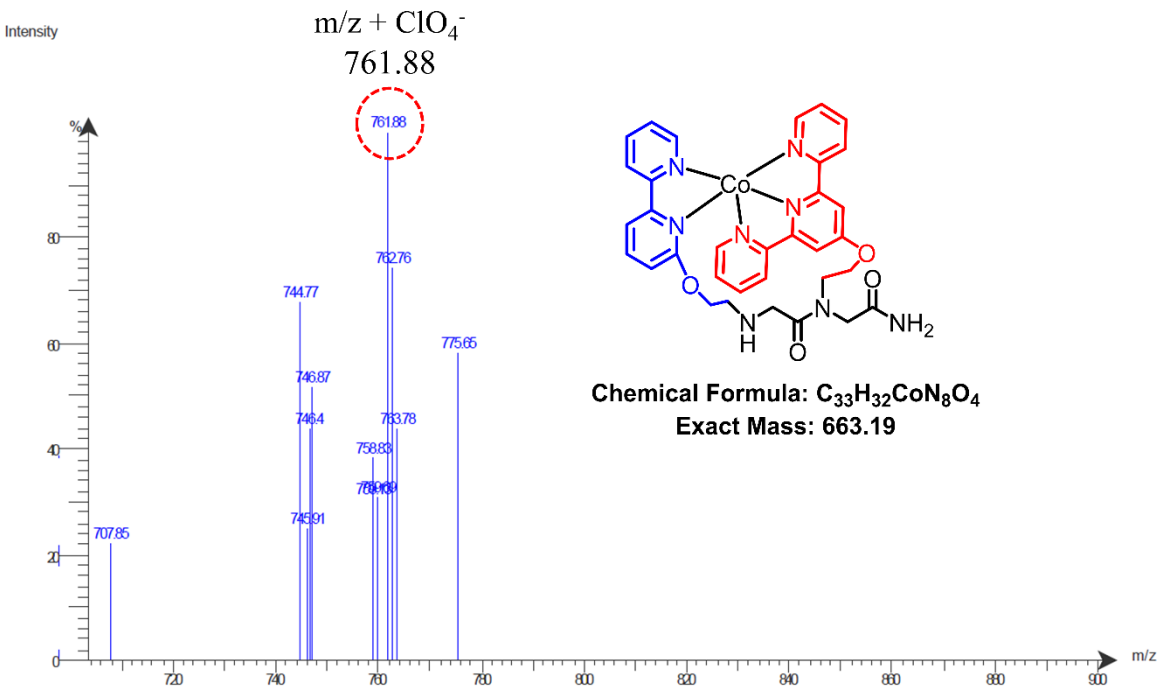

Figure S64. ESI-MS of peptoid Co**TB**.

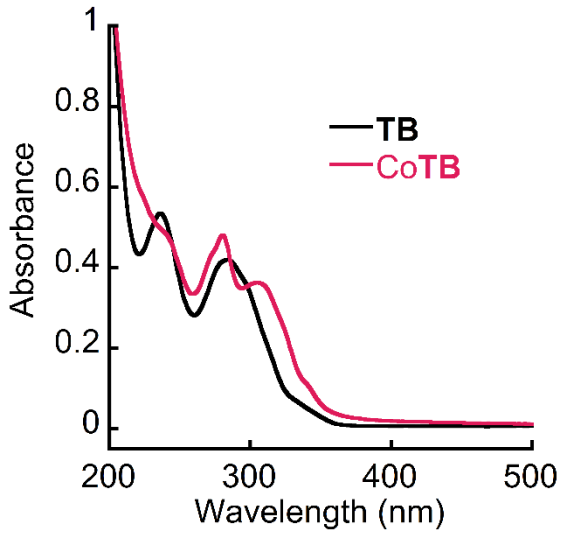

Figure S65. UV-Vis spectra of 25 µM of the peptoid **TB** and complex Co**TB** in PBS at pH 7.

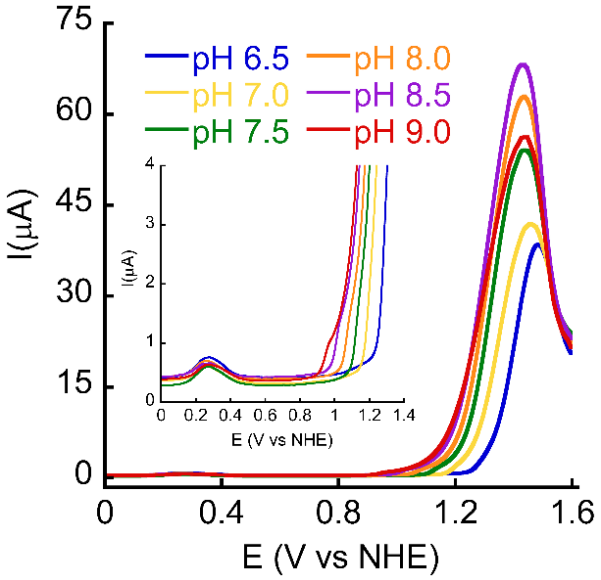

Figure S66. DPVs of Co**TBE** in 0.1M phosphate buffer at pH range between 6.5 to 9 (scan rate =20 mV/s).

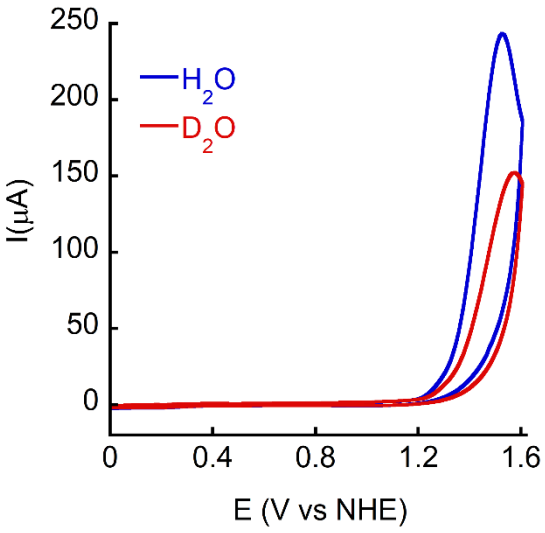

Figure S67. CVs of 0.5mM Co**TBE** in H_2O and D_2O in 0.1 M PBS at pH 7.0 (scan rate 100 mv/s).

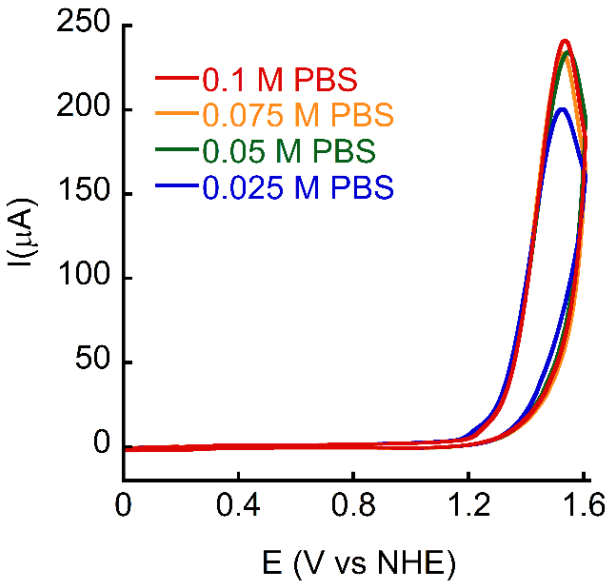

Figure S68. CVs of 0.5mM Co**TBE** in different concentrations of phosphate buffer at pH 7, the ionic strength was maintained by adding KNO_3 (scan rate 100 mv/s).

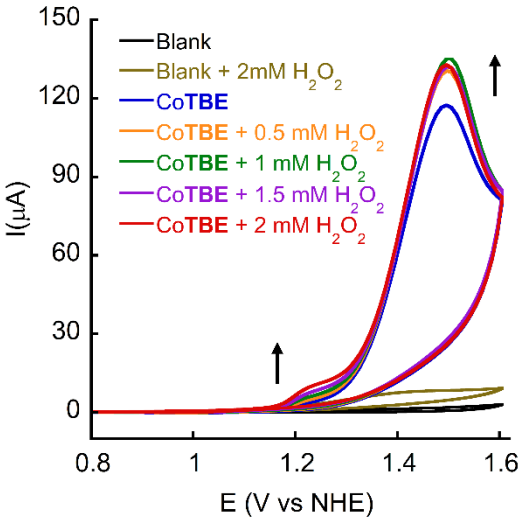

Figure S69. CVs of 0.5mM Co**TBE** in 0.1M phosphate buffer at pH 7 with the increasing concentration of H_2O_2. (Scan rate = 10 mV/s).

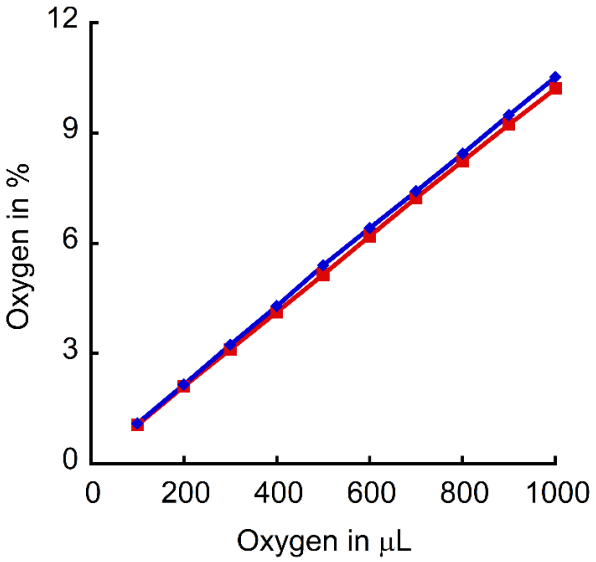

Figure S70. Calibration curve for the measure of evolved O_2 in μL from %. [Red line = experiment 1 and blue line = experiment 2 and then take the average].

$$\frac{i_{cat}}{i_p} = \frac{n \cdot 2.24\sqrt{\frac{RT \cdot K_{obs}}{F\nu}}}{1 + \exp\left[\frac{F}{RT} \cdot (E_{cat} - E)\right]}$$

Equation S1: The formula used to obtain kobs by Foot-of-the-wave analysis (FOWA):[6]
• Ecat – the standard potential for the catalysis-initiating redox couple calculated from DPV.
• icat – the catalytic current intensity in the presence of substrate.
• ip – the non-catalytic current intensity.
• n=4 (for water oxidation) the number of electrons in the reaction.
• F=96485 C/mol, R=8.314 J/mol•K, T=298K, ν – scan rate in V/s.

Table A1. Data summary of Co-based electrocatalysts for homogeneous water oxidation in aqueous media from reported literature

Catalyst	**Overpotential** [a]	**pH**	**Buffer solution**	**K_{cat}**	**Coordination type**	**Total hours of CPE experiment performed**	**Stability** [d]	**Reference**
Co (bipyalk) $(OAc)_2$	~520	6	0.1M Phosphate buffer	1.5[b]	Intramolecular	2.5 hrs	√	7
$[Co(TCA)_2 \cdot 2H_2O]$	~520	6	0.1M sodium Acetate buffer	-	Intermolecular	11 hrs	Deposition of Molecular catalyst observed	8
Co**TBE**	~430	7	0.1M Phosphate buffer	44[c]	Intramolecular	10 hrs	√	This work
$CoH^{\beta F}CX–CO_2H$	780	7	0.1 M Phosphate buffer	0.81[c]	Intramolecular	1 hr	√	9
vitamin B12	~880	7	0.1 M aqueous NaPi buffer	-	Intramolecular	11 hrs	√	10
$Na[(L_1{}^{4-})Co^{III}]$	780	7	0.1 M Phosphate buffer	7.53[c]	Intramolecular	~1 hr	√	11
$[(TPA)_2Co_2\text{-}(\mu\text{-}OH)\ (\mu\text{-}O_2)](ClO_4)_3$	540	8	0.1 M Borate buffer	~1.4[b]	Dinuclear (Intermolecular)	3 hrs	Formation of Co-Oxide observed	12
$[Co^{III}(dpaq)(Cl)]$	740	8	0.1 M Phosphate buffer	85[c]	Intramolecular	~3 hrs	√	13
$[Co^{III}(dpaq)(OH)]ClO_4$	640	8	0.1 M Phosphate buffer	75.6[c]	Intramolecular	~3 hrs	√	14
$[Co(bpbH_2)Cl_2]$	~770	8.6	0.25 M buffer	81.54[c]	Intramolecular	5 hrs	√	15
$[Co(N_3Py_2)(H_2O)](ClO_4)_2$	750	9.0	0.1 M Borate buffer	0.79[c]	Intramolecular	~1 hr	√	16
TPT$_2$-Co^{III}	500	9.0	0.1 M Phosphate	108[c]	Intermolecular	10 hrs	√	17
$[Co^{II}(Py_5)(OH_2)]$	~900	9.2	0.1 M Phosphate buffer	79[c]	Intramolecular	~0.15 hrs	√	18
$(Et_4N)[(Co^{III}\text{-}bTAML)]$	~810	9.2	0.1 M Phosphate buffer	5.8	Intramolecular	3 hrs	√	19
$[Co(N2Py3)](ClO_4)_2$	~970	11	0.1 M Phosphate	0.23[c]	Intramolecular	4 hrs	√	20

a: all the reported potentials are approximate based on CPE experiment performed, b: measured by experiments, c: calculated by Randles-Sevcik equation, d: stability in solution after CPE, √ : Stable as molecular catalyst.

References:

1. G. Maayan, B. Yoo, K. Kirshenbaum, Tetrahedron Lett 50 (2009) 4297-4297.
2. Baskin, M.; Panz, L.; Maayan, G. *Chem. Commun.,* **2016**, *52*, 10350-10353.
3. T.W. Green and P.G.M. Wuts, Protective Groups in Organic Synthesis, Wiley-Interscience (1999) 127-141 708-711.
4. R. N. Zuckermann, J. M. Kerr, S. B. W. Kent, W. H. Moos, *J. Am. Chem. Soc.* **1992**, *114*, 10646–10647.
5. P. K. Das, S. Bhunia, P. Chakraborty, S. Chatterjee, A. Rana, K. Peramaiah, M. M. Alsabban, I. Dutta, A. Dey and K.-W. Huang, *Inorg. Chem.*, 2021, **60**, 614 -622.
6. 32 (a) C. Costentin, S. Drouet, M. Robert, J. M. Savéant, *J. Am. Chem. Soc.* 2012, **134**, 11235–11242. (b) C. Costentin, J. M. Savéant, ChemElectroChem, 2014, **1**, 1226-1236;
7. Yun-F. Su, Wen-Z. Luo, Wang-Q. Lin, Yi-B. Su, Zi-J. Li, Yong-J. Yuan, Jian-F. Li, Guang-H. Chen, Z. Li, Zhen-T. Yu, and Z. Zou, *Angew. Chem. Int. Ed.* **2022**, *61*, e202201430.
8. H. A. Younus, N. Ahmad, A. H. Chughtai, M. Vandichel, M. Busch, K. V. Hecke, M. Yusubov, S. Song, and F. Verpoort ChemSusChem 2017, 10, 862 – 875
9. D. K. Dogutan, R. McGuire and D. G. Nocera, *J Am Chem Soc*, 2011, **133**, 9178-9180.
10. H. M. Shahadat, H. A. Younus, N. Ahmad, S. G. Zhang, S. Zhuiykov and F. Verpoort, *Chem Commun*, 2020, **56**, 1968-1971.
11. Hao-Y. Du, Si-C. Chen, Xiao-J. Su, L. Jiao, and Ming-T. Zhang, J. Am. Chem. Soc. 2018, 140, 1557−1565
12. (a) H. Y. Wang, E. Mijangos, S. Ott and A. Thapper, *Angew. Chem. Int. Ed.*, 2014,**53**, 14499-14502, (b) J.-W. Wang, P. Sahoo and T.-B. Lu, ACS Catal., 2016, 6, 5062.
13. S. Biswas, S. Bose, J. Debgupta, P. Das and A. N. Biswas, *Dalton Trans*, 2020, **49**, 7155-7165.
14. P. Lepcha, S. Biswas, S. N. Chowdhury, S. Bose, J. Debgupta, S. Paul, and A. N. Biswas *Eur. J. Inorg. Chem.* 2023, *26*, e202200611
15. Z.-Q. Wang, L.-Z. Tang, Y.-X. Zhang, S.-Z. Zhan and J.-S. Ye, J. Power Sources, 2015, 287, 50.
16. H. Zheng, H. Ye, T. Xu, K. Zheng, X. Xie, B. Zhu, X. Wang, J. Lin and Z. Ruan; *New J. Chem.*, 2022, 46, 7522–7527.
17. G. Ruan, L. Engelberg, P. Ghosh and G. Maayan, *Chem. Commun.*, 2021, 57, 939-942.
18. D. J. Wasylenko, C. Ganesamoorthy, J. Borau-Garcia and C. P. Berlinguette, *Chem Commun*, 2011, **47**, 4249-4251.
19. D. Das, S. Pattanayak, K. K. Singh, B. Garai and S. Sen Gupta, Chem. Commun., 2016, 52, 11787
20. Y. Chen, X. Meng, X. Chen, X. Li, H. Ye, S. Liu, Z. Ruan, X. Liang and J. Lin Sustainable Energy Fuels, 2023, 7, 242–247